Geomorphology 450 (2024) 109082

Contents lists available at ScienceDirect

Geomorphology

journal homepage: www.journals.elsevier.com/geomorphology

Assessment of piping-sinkhole development in a fluvial-terrace scarp retreat environment: A multi-temporal analysis on the lower Ticino River (Italy)

A. Bosino [a,*], A. Mandarino [b,c], M. De Amicis [a], F.F. Cazzini [d], D. Abu El Khair [a], P. Flores [d]

[a] Department of Earth and Environmental Sciences, University of Milano-Bicocca, Piazza della Scienza 1, 20126 Milano, Italy
[b] Department of Earth, Environment and Life Sciences, University of Genova, Corso Europa 26, 16132 Genova, Italy
[c] Geoscape Geo-Environmental Consulting, Spin-Off of the University of Genova, Via Varese 2, 16122 Genova, Italy
[d] Freelance researchers

ARTICLE INFO

Keywords:
Fluvial Terrace
Scarp Piping-Sinkhole (SPS)
Geomorphological survey
Ticino River

ABSTRACT

This paper investigates, from a geomorphological and hydrogeological point of view, the development of piping-sinkhole phenomena at a retreating fluvial-terrace scarp along the lower Ticino River, near Casottole, northern Italy. Piping forms and features are well documented in the literature as complex soil erosion phenomena, usually associated with clayey or carbonate substrata, or to specific fluvial deposits. Such phenomena appear to have never been mapped in the lower Ticino area, and up to now, no evidence of piping-sinkhole occurrence in terraced alluvial plains strictly associated with terrace scarp erosion processes have been observed and reported in the literature. The geomorphological peculiarities of the area were assessed through field surveys, photographic and drone imaging, photointerpretation, and GIS analysis. Moreover, the riverbed morphological evolution was evaluated since the 1950s, and the hydrogeological conditions were analysed. Finally, a large piping-sinkhole database composed by 35 landforms was assembled in a WebGIS system. The piping-sinkhole phenomena were associated with the presence of perched water tables with flows towards the Ticino River, whose origin can be associated with site conditions, the large up dip network of surface water, and local irrigation practices. The research presented here provides a new contribution to the understanding of sinkhole occurrence and formation in previously unstudied terrace-scarp settings, and new insights for fluvial-terrace scarp modelling. Furthermore, it represents an important knowledge base to inform sustainable and effective measures for environmental management and hydrogeomorphic risk mitigation with reference to terrace scarp erosion and sinkholes.

1. Introduction

The term “sinkhole” has historically been associated with karst terrains, as a synonym of the term “doline” (Fairbridge, 1968; Monroe, 1970; Bates and Jackson, 1983; Wilson and Moore, 1998; Williams, 2004; Waltham et al., 2005; Sharp, 2016). However, it has successively been applied to any form of mainly circular surface depression or collapse structure, measuring a few to tens or hundreds of meters in diameter, irrespective of the nature of the underlying bedrock or of the genetic processes involved, leading to some confusion as described by several authors (e.g., Beck, 1984; Beck and Wilson, 1987; Nisio, 2003). Currently, the term is used in this sense, preceded where possible by a qualifier indicating its genesis (e.g., solution sinkhole, collapse sinkhole, piping-sinkhole etc.). Sinkholes can be anthropogenic or natural in origin and their often-sudden appearance can represent a major hazard in populated areas (e.g., Parise et al., 2013; Parise and Vennari, 2013; Strzałkowski, 2019).

Due to the impact of sinkholes on the environment and on human activities, many studies have been carried out, focusing on the geological conditions leading to their formation. The scientific literature on sinkholes is therefore abundant and varied and describes phenomena occurring in various parts of the world and in different geological

Abbreviations: Ahe/IB, anabranching (high energy)/island-braided; Ahe, anabranching (high energy); AI, anabranching index; BI, braiding index; CA, channel area; CL, channel length; CP, channel pattern; CP – BRT, channel pattern - basic river typologies; CP – ERT, channel pattern - extended river typologies; CW, channel width; DB, database; DPS, deep piping-sinkhole; KSat, saturated hydraulic conductivity; L, downstream-most stratigraphic profile; LS, landslide scar; M, upstream-most stratigraphic profile; PS, piping-sinkhole; SI, sinuosity index; SPS, scarp piping-sinkhole; SVS, steep to sub-vertical scarp; W, wandering.

* Corresponding author.
E-mail address: alberto.bosino@unimib.it (A. Bosino).

https://doi.org/10.1016/j.geomorph.2024.109082
Received 1 August 2023; Received in revised form 19 January 2024; Accepted 23 January 2024
Available online 28 January 2024

environments. This literature includes extensive reviews and landform modelling approaches (e.g., Beck, 1984; Tharp, 1997; Waltham et al., 2005; Nisio et al., 2007; Nisio, 2008; La Vigna et al., 2013; Gutiérrez, 2016; La Vigna, 2016; Bianchini et al., 2022). Furthermore, Nisio and Salvati (2004) and Nisio et al. (2007) report a collapse classification proposal based on the genesis, propagation mechanism and triggering type of these phenomena, highlighting that most sinkholes are related to chemical dissolution of subsurface rocks, but others can be related to physical erosion in the subsurface by underground water flow.

In Italy, an effort to inventorize and systematically classify sinkholes based on their genesis was initiated in 2002 under the auspices of the Italian Institute for Environmental Research and Protection (ISPRA) and conducted by the Italian Geological Survey – APAT (ISPRA, il Progetto Sinkholes – https://www.isprambiente.gov.it). Among the many contributors to this effort, Nisio (2003, 2008), Nisio and Salvati (2004), Nisio et al. (2007), Caramanna et al. (2008), and other authors highlighted the importance, besides karst phenomena, of suffusion and piping processes in the generation of sinkholes. The term suffusion indicates the removal of finer particles in the subsurface by underground water seepage, resulting in the loss of mass and increase of hydraulic conductivity. In this process there can also be significant loss of volume (creation of voids), which can lead to the collapse of the overburden (Fannin and Slangen, 2014).

The term soil piping or piping (Parker, 1964) describes a process whereby subsurface water flow in soils or poorly consolidated sediments can concentrate in a system of underground "pipes" which erode and remove the enclosing material (e.g., Bernatek-Jakiel and Poesen, 2018 and references therein) impacting on environment and society (Bernatek-Jakiel and Nadal-Romero, 2022). As specified by Jones (1994) piping evidence can be found in all climatic regions. The term piping is referred in general to seepage erosion, suffusion and pipeflow mechanisms of subsurface flow erosion (Wilson et al., 2018). In Italy for example piping processes are associated with particularly fine-grained bedrock, e.g. the Varicoloured clays of Cassio and other geological formations which crop out in several parts of the Apennines (e.g., Ciccacci et al., 2008; La Licata et al., 2023) and are able to trigger gully and process erosion processes (Bryan and Yard, 1982; Jones, 1994; Bosino et al., 2019). In general, the role of the piping processes in gully development is well known (e.g., Wilson, 2011; Bernatek-Jakiel and Wrońska-Wałach, 2018; Wilson et al., 2018 and reference therein). Moreover, piping processes have been observed and correlated both with streambanks and shorelines in many parts on the world (Berry, 1970; Jones, 1971; Hagerty, 1991 and reference therein). Piping processes have been linked with alluvial deposits characterized by the alternation of fine and coarse deposits, but also in glacial terrains or in more general in heterogenic terrain characterized by alternations of fine and coarse layers with joins and fractures allowing water infiltration and flows. In Italy, collapse structures with a polygenic origin are the so called "Occhi Pollini" sinkholes which have caused considerable damage in residential areas. These landforms are related to fluvio-glacial deposits with a large carbonate component and to unconsolidated alluvial deposits (Strini, 2004; Colombo et al., 2015). These landforms present different dimensions and are related both to chemical dissolution of carbonatitic block present in conglomeratic formations (e.g., the Ceppo) or triggered by piping processes due to interstratified layer of glacial and fluvio-glacial deposits which act as impermeable layers below permeable colluvial deposits.

Sinkholes generated by a combination of dissolution and piping processes have been described in Italy in different geological contexts (Nisio et al., 2008). In several examples where a thick sedimentary section overlies a carbonate substratum, uprising fluids from cavities or fractures in the carbonate bedrock have been shown to cause upward propagation of cavities by roof collapse (deep piping-sinkholes or DPS described by White (1988), Nisio et al. (2008), Caramanna et al. (2008)). In general, these piping-sinkholes are polygenic landforms, commonly associated with alluvial sediments characterized by vertical and horizontal granulometric variations that lie on karst bedrock (Nisio et al., 2007; Nisio et al., 2008; Cardarelli et al., 2013). The karstification of carbonate bedrock causes cavities that extend from the bedrock into the upper deposits until the alluvial material collapses create the piping-sinkhole landforms. Although the majority of piping-sinkholes in Italy are associated with carbonate sediments (Nisio et al., 2007) some examples have been described in alluvial plain environments in the absence of carbonate rocks, where groundwater flow above a relatively impermeable substratum caused the erosion of the alluvial sands and silts generating the collapse of the overlying terrain in the form of sinkholes (e.g., Del Prete et al., 2008; Dell'Aringa et al., 2013). Similar processes have been described and modelled in alluvial deposits of the Dead Sea area by Al-Halbouni et al. (2018). Other examples of pipe-collapse landforms directly associated with alluvial plain deposits as well as stream deposits have been reported by Berry (1970), Jones (1971) and Zhang and Wilson (2013). Specifically, Berry describes sinkholes which form on the fluvial terraces of the Butana (Sudan) due to underground water movement and associated piping after increased irrigation in the dry season provides the necessary hydraulic gradient towards the Nile banks.

However, to the best of our knowledge no evidence for piping-sinkholes directly associated with terrace scarp erosion processes, hence with riverbed migration, has been observed and reported in the literature. Several studies have investigated riverbank erosion phenomena (e.g., Hagerty et al., 1981; Thorne and Abt, 1993; Rinaldi and Casagli, 1999; Dapporto et al., 2003; Clark and Wynn, 2007; Mandarino et al., 2021a). However, works focusing on the retreat of fluvial-terrace scarps are absent. Processes that act on either a retreating bank or a retreating scarp of fluvial terrace can be both erosion processes, namely, seepage and particle-by-particle detachment caused by flowing water, and mass failure associated with the action of gravity (Hooke, 1979; Rinaldi et al., 2015a). Floods may induce the development of perched water tables and subsequently rapid subsurface flows to streams during the flooding recession (Hagerty, 1991; Rinaldi et al., 2004; Wilson et al., 2007, and references therein). These subsurface waters emerging at a riverbank have potential for erosion and may contribute to gully formation (Römkens et al., 1997; Froese et al., 1999) and bank retreat (Dunne, 1990) through seepage erosion. According to Dunne (1990), such erosion begins from the downstream end of a subsurface flow path and extends headward, often resulting in cavities that promote bank failure (Simon et al., 1999; Wilson et al., 2007; Okeke et al., 2020).

Against this background, this study, conducted in the surroundings of the village of Casottole (northern Italy) (Fig. 1), investigated the development of piping-sinkhole phenomena over the fluvial terrace in close proximity to the retreating fluvial-terrace scarp brushed by the Ticino River and over the scarp itself. This area is characterized by a great relevance in terms of nature conservation, landscape beauty, agriculture, and outdoor recreational activities.

A significant geomorphic instability associated with riverbed lateral migration and consequent fluvial terrace scarp erosion and piping-sinkhole formation have affected the study area over the last decades shaping very unusual landforms. Piping-sinkholes have not previously been described along the Ticino River and no other sites along this fluvial system present such landforms. Furthermore, the presence of scattered piping-sinkholes as well as the local collapse of the retreating fluvial-terrace scarp are elements of hydrogeomorphic hazard and risk. For these reasons this research aims to: (i) investigate the piping-sinkhole formation processes, (ii) document for the first time piping-sinkhole formation associated with fluvial-terrace scarp retreat, (iii) outline the recent geomorphological evolution of the study site in a land management and hydrogeomorphic risk reduction perspective and (iv) introduce novel elements for the classification and understanding of sinkhole phenomena worldwide.

In this study it has been possible to reconstruct the evolution of the scarp in the last twenty years through field and drone observations as well as the analysis of photographs and Google Earth images covering

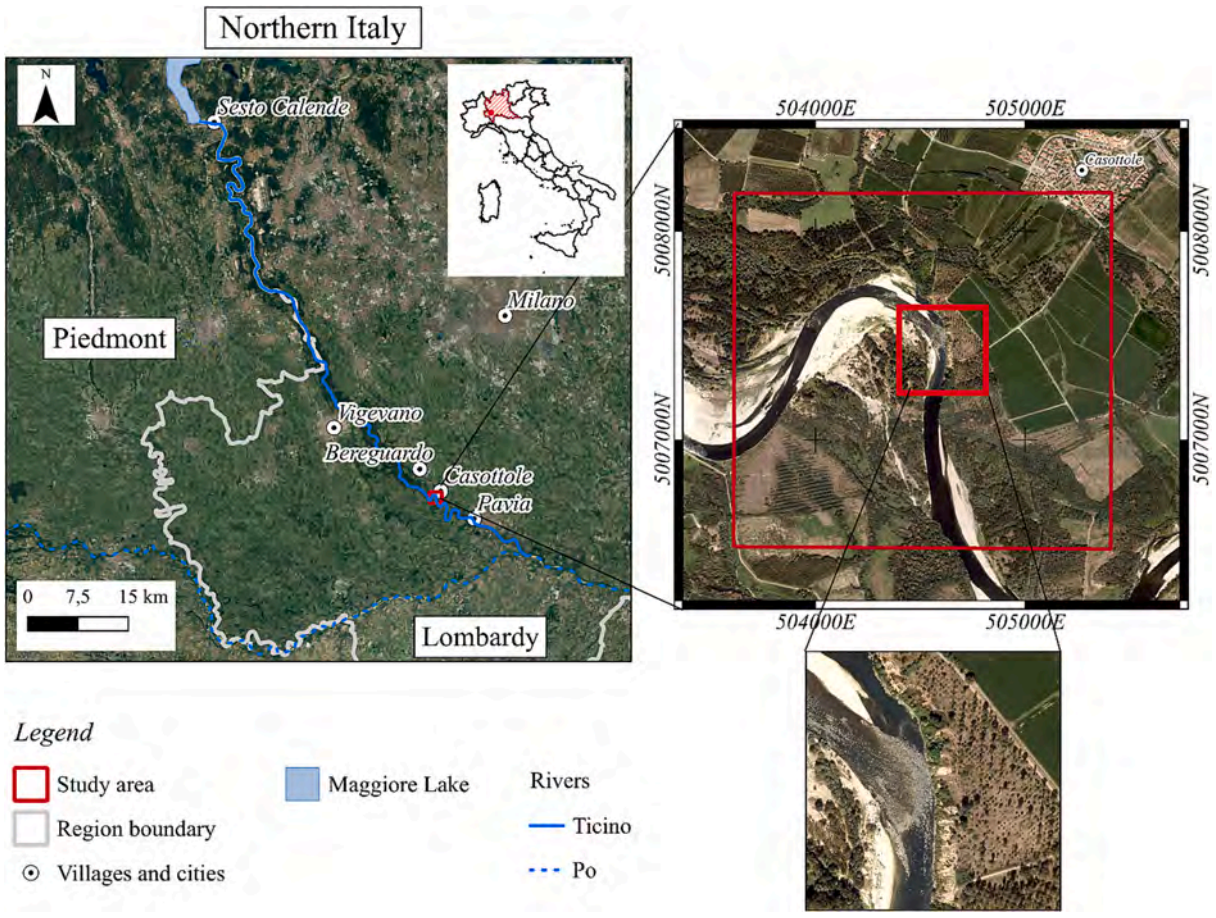

Fig. 1. Study area showing the river bend and river scarp where piping-sinkholes are developed. Basemap: on the left Google Satellite image year 2016, on the right orthophoto year 2018 from Lombardy Region public database, https://www.geoportale.regione.lombardia.it/.

the whole period. The study was also complemented by a regional geological and hydrological assessment based on available stratigraphic and well data, and dedicated field surveys. The particular position of the piping-sinkholes observed in the study area, i.e. on the Ticino River terrace and scarp, suggests an influence of fluvial processes in their formation and evolution. The morphological adjustments of the Ticino River were evaluated at both the reach and site scale through the multi-temporal GIS analysis of data covering the last 70 years. Finally, a piping-sinkhole database, correlated with the scarp edge position, was established and the historical evolution of the area was reported in an ad hoc WebGIS integration.

2. Study area

The study area is sited on the left bank of the Ticino River west of the village of Casottole in the Torre d'Isola Municipality, Lombardy Region, northern Italy (Fig. 1). The area is also located within the Ticino River Natural Park, with protection according to the Natura 2000 European Network. It represents one of the most striking landscapes in the monotonous lowlands of the Po Plain, since the river flows are semi-confined, incising the fluvial terrace deposits to produce a topographic scarp of roughly 20 m. Climatically, the study area falls in the Cfa classes (warm temperate climate, fully humid with hot summer) according to the Köppen climate classification (Kottek et al., 2006). The area experiences an average rainfall of 825 mm/yr (Ceriani and Carelli, 1999) and is sited in a rural context of farm and agricultural fields where recreational paths and nature trails are developed close to the river. From a regional perspective the Po Plain is a flat alluvial plain underlain by several stratified layers of Plio-Pleistocene marine, fluvio-glacial and fluvial sediments (Servizio Geologico d'Italia, 1967). At present, the Ticino River along its valley displays overall a wandering channel pattern from Lake Maggiore to Casottole, with several narrow secondary channels, bars, and islands. Downstream of Casottole the riverbed is characterized by a sinuous single thread channel with some meanders up to the Po River confluence (Fig. 1). The riverbed comprises sand and pebble sediments. The whole course of the Ticino River downstream of Lake Maggiore presents a hydrological regime conditioned by severe anthropic pressures, such as the regulation of the outflow from the aforementioned lake and the exchange of water flows with a dense and complex network of diversion and tributary channels (AdBPo, 2001). Furthermore, in-channel sediment quarrying, and channelization affected the riverbed over the 20th century, as documented along other Italian rivers (e.g., Marchetti, 2002; Surian et al., 2009; Scorpio et al., 2015). No detailed information on active channel vertical changes is available and an overall reduction of the riverine area, associated with the natural and anthropogenic abandonment of secondary channels was documented over approximately the last 150 years (Consorzio Parco Ticino, 1998). However, unlike most Italian rivers, some reaches still present a very low channelization, with natural banks, secondary channels, and active lateral migration processes. Several levels of fluvial terraces are present in the lower part, between the current alluvial plain and the "Main Level of the Plain" (Marchetti, 2002) which represents the surface of maximum aggradation of fluvio-glacial and fluvial sediments reached in the Pedealpine Plain during the Last Glacial Maximum.

In the study area, the Ticino river's left bank juxtaposes the river and one of the highest terraces, with a difference in elevation of about 20 m. The study area corresponds to the fluvial-terrace scarp eroded by the Ticino River over the last decades and its surroundings (Fig. 1). This is a

confined concave side of a riverbed bend largely affected by erosional processes (Fig. 2a, b). The scarp is characterized by an alternation of heterometric gravel and sand layers, interbedded with finer-grained fluvial deposits. The granulometry as well as the observed sedimentary structures (e.g., cross bedding stratification) varies laterally along the exposed section. These deposits lie on the top of a continuous grey basal silty level. On the opposite (convex) side there is a large point-bar attached to the bank (Fig. 2c). In the upper and lower parts (N and S) of the study site scarp toe erosion triggers rockfalls causing a sub-vertical scarp (SVS) retrogression (Fig. 2a and b). In addition, on the top of the oldest river terraces, directly facing the river, sub-circular piping-sinkholes can be mapped (Fig. 2d and e). Finally, in the central-northern part of the area and locally in the southern part, large sub-circular niches can be observed where the fluvial deposits crop out in the riverbank (Fig. 2e), which are directly associated to the fluvial-terrace scarp.

From a hydrogeological perspective the area is characterized by several confined and semiconfined aquifers, overlain by permeable layers in which the aquifer flows unconfined (Pilla, 2010). The aquifers show a steep overall gradient from the eastern part of the study area to the river bed (Lombardy Region public database, https://www.geoportale.regione.lombardia.it/). Focussing on the fluvial terrace scarp local water springs can be observed, which can be related to the alternation of fine and coarse layers representing different depositional events. Although no carbonate bedrock is present, the scarp stratification causes a significant local textural variability with perched groundwater, able to trigger piping phenomena leading to the formation of piping-sinkholes.

The morphological evolution of the area considered in this study is closely connected to subsurface and runoff associated processes (e.g., piping and rill-interrill evidence) as well as to slope collapse and scarp erosion due to the Ticino River. The balance between these processes determines the activation of local piping-sinkholes or the stabilization of portions of the terrace scarp (Fig. 2d and e). The piping-sinkhole development is related to subsurface water movement able to produce

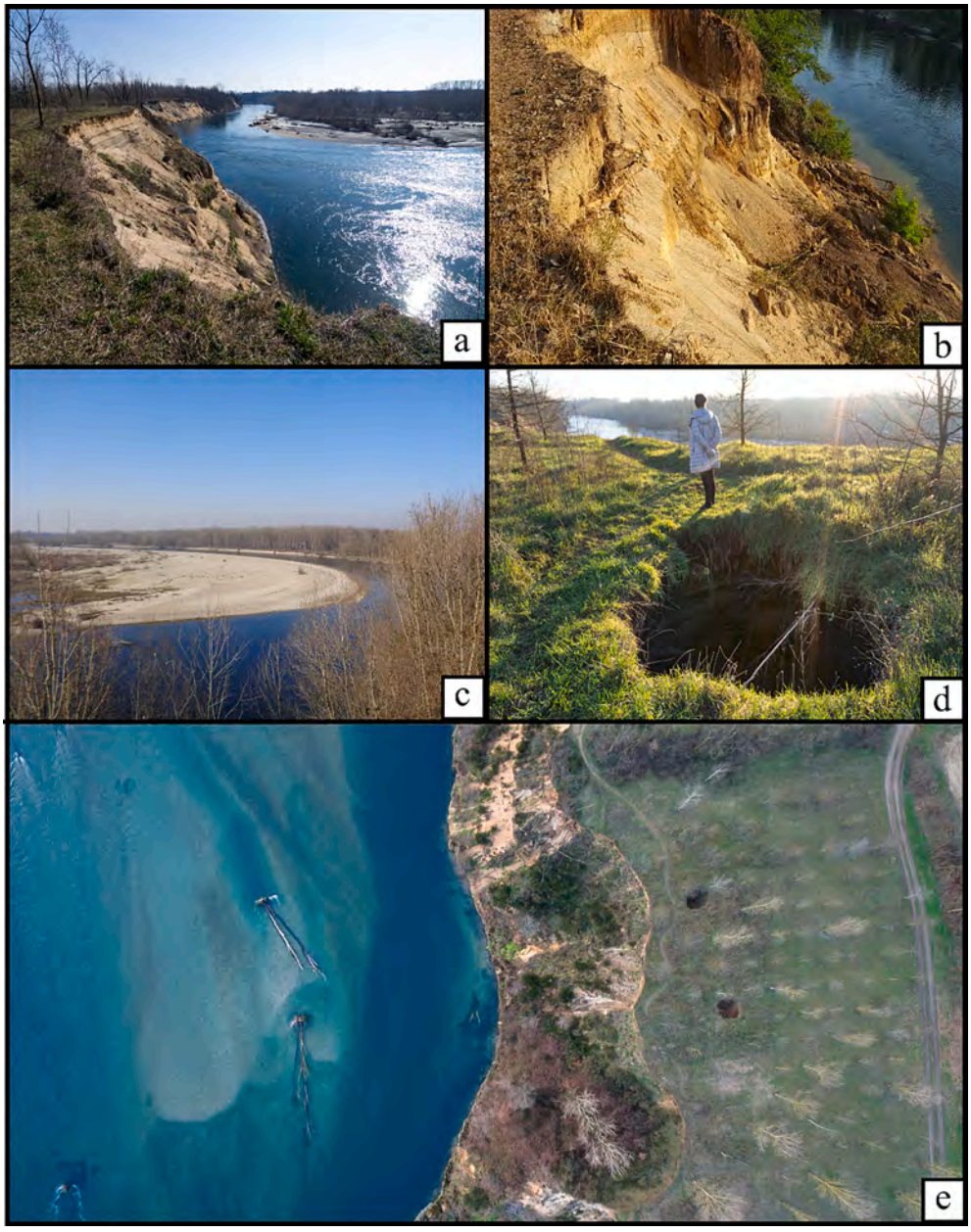

Fig. 2. Landforms in the study area. (a): The Ticino River and retreating fluvial-terrace scarp. (b): Stratified sediments and slope instability evidence. (c): Point-bar. (d): Piping-sinkhole. (e): Drone view from above showing piping-sinkholes on the top of the terrace and associated to the terrace scarp.

sub-erosion, creating voids that collapse producing sinkholes. The dimensions of the landforms are variable and depend on the depth and the power of the piping phenomena. The piping-sinkhole processes complement the scarp-toe erosion which triggers slides and debris fall (Fig. 2a). In this case the scarp is steep to sub-vertical (SVS) and slope associated processes are the main modelling elements.

3. Materials and methods

The methodology followed to assess the morphological evolution of the area (Fig. 3) is based on fieldwork including geomorphological observations and mapping as well as field measurements, realization of hydrogeological cross-sections and finally laboratory and GIS analyses.

3.1. Landforms identification and characterization

The nature and relation between the different morphological elements present in the study area, their morphometric characteristics and their evolution were studied through the analysis of field observations carried out in the last years and integrated with original photographic documentation acquired since 2004, original drone imaging acquired from 2015, and public domain Google Earth images. The latter are freely available for the years 2007, 2012, and 2014–2023.

The key landforms identified were attributed to 3 main morphotype classes (see Results section) namely Piping-Sinkholes (PS), Scarp Piping-Sinkholes (SPS) and Landslide Scars (LS) and named with a numerical identifier roughly correlated with their sequence of formation. A few

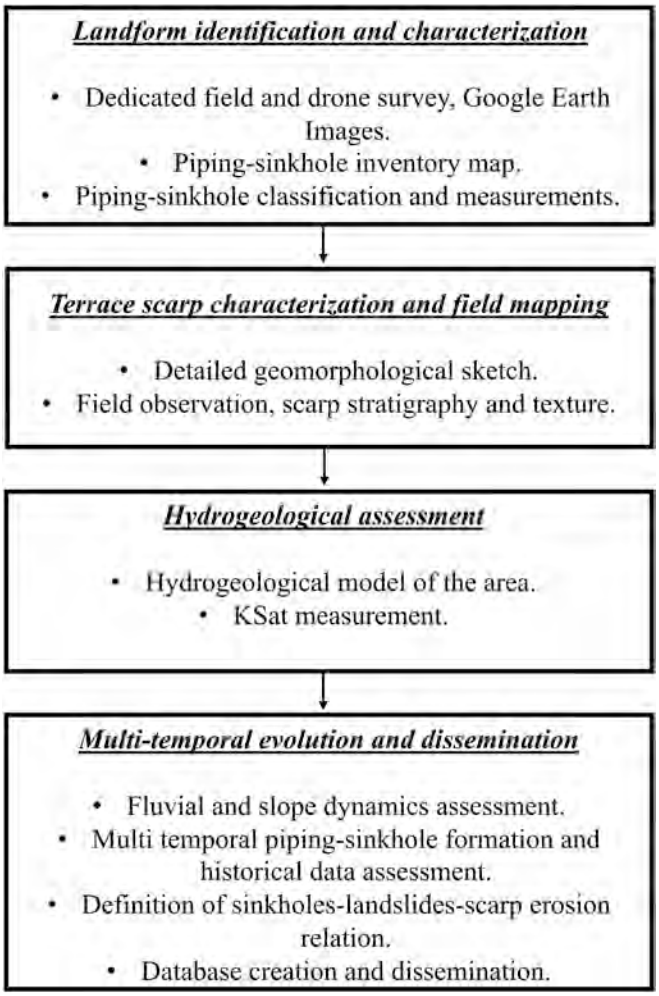

Fig. 3. Flowchart explaining the adopted methodology.

SPSs were named with a letter identifier (X, Y, Z). The landforms were characterized as follows: (a) PS: coordinates of centre, diameter and depth measured from ground level, (b) SPS: diameter of circle drawn on terrace surface by the sinkhole rim, coordinates, and depth from terrace level of circle centre, (c) LS: diameter and centre coordinates of circle drawn on the terrace surface by the scar. Smaller landforms (PS) were measured in the field, while larger, inaccessible or past/eroded ones were estimated from photographs and drone/Google Earth images. For each landform the time of formation and/or earliest recorded date was also derived from available documentation such as image metadata or other observations. The drone used was a DJI Phantom 3 PRO with a 20 mm (35 mm equivalent) lens with 94° field of view and a 12.4 M pixel sensor with 4 K video resolution. Accurate GPS positioning enabled precise tracking and recording of image point of view. Images were processed with standard image processing software.

3.2. Terrace scarp characterization and field mapping

Two high-resolution geomorphological scarp sketches were drawn in order to map active landforms and understand the fluvial-terrace scarp evolution. The geomorphological outlines were produced adapting the Italian guidelines for the geomorphological cartography (Campobasso et al., 2021). The symbols were drawn on high-resolution drone images dated March 2017 and September 2017 and the geomorphological output verified with several field excursions during 2022 and 2023. The second step was a comprehensive analysis of the lithological and the morphological characteristics of the study site. The lithological characteristics of the sedimentary layers which compose the terrace scarp were determined using two detailed stratigraphic columns surveyed in the field that were drafted in correspondence of both SPS and SVS outcrops in order to understand: (i) the lithology of the scarp, (ii) the lithological influence on the scarp erosion and associated scarp slope processes and (iii) the relation between sedimentary layers and scarp piping-sinkhole formation. For each detected layer soil samples were collected, and texture analyses were done in the Milano-Bicocca University laboratory. Soil samples were analysed using the pipette method (wet sieving and sedimentation; standard ISO 11277:2020) and the results were plotted on Shepard triangular diagram (Shepard, 1954).

3.3. Hydrogeological assessment

As documented in the literature (e.g., Farifteh and Soeters, 1999; Nisio, 2008; Bovi et al., 2020), sub-horizontal pipes are guided by subsurface water flow in permeable layers overlying low-permeability ones. Field observations on the terrace scarp confirm the presence of water springs associated with low or reduced permeability layers, and a hydrological assessment was deemed necessary to understand the correlation between subsurface water flow, lithology, and piping development, directly linkable with PS and SPS formation, as well as to verify the more regional presence of low-permeability layers observed at site scale, and their interaction with subsurface water flow. Two hydrological sections (Fig. 4) were thus constructed, taking into consideration the scarp stratigraphy data assessed in the 25-02-2023 and 25-3-2023 field surveys, with particular attention to the presence of relatively impervious layers, the regional stratigraphy of the area established by previous studies (Pilla, 2010) and the available Lombardy Region public database (https://www.geoportale.regione.lombardia.it/) on which the main hydrological data of the existing water wells have been recorded.

The altitude of the river, river terrace and other well points were derived from the topographic maps and compared with LIDAR data 1 m resolution from Lombardia regional geoportal (https://www.geoportale.regione.lombardia.it/).

Finally, to evaluate the superficial infiltration capacity of the topsoil different saturated hydraulic conductivity (KSat) measurements were conducted on the top of the terrace using a constant head-permeameter (Amoozegar, 1989; Bettoni et al., 2023). Three representative PS

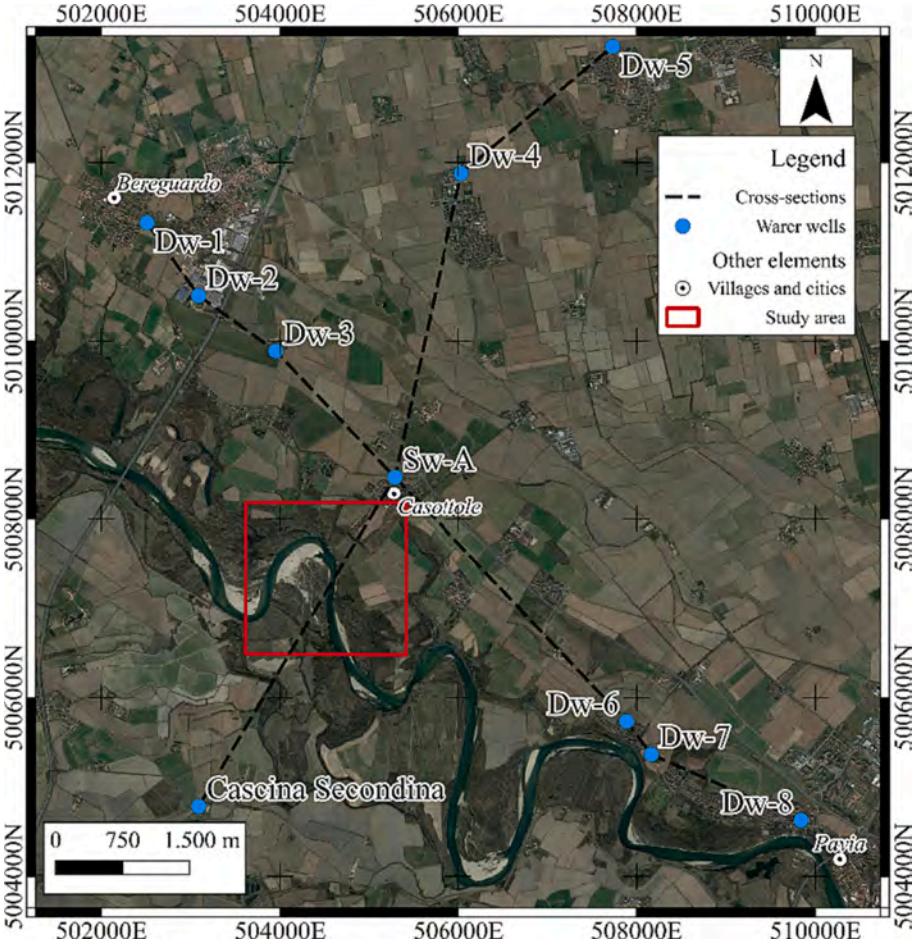

Fig. 4. Location of water wells stratigraphy and data utilized for the layer correlation at regional scale. Dotted lines represent the position of the cross-sections a and b of Fig. 9-result section. Basemap: Google Satellite image year 2016.

landforms were selected (PS 7, PS 11 and PS 12) in order to distribute the measurements within in the main area of PS development. Two KSat tests were conducted for each PS (six measurements) and the results mediated.

3.4. Multi-temporal evolution and dissemination

A multi-temporal reconstruction of the PS, SPS, and scarp evolution, along with the Ticino riverbed morphology and dynamics, was performed starting from available data and historical observations. To evaluate the potential influence of the Ticino River morphodynamics on piping-sinkhole activation, the Ticino River planform changes were analysed at both reach and site scale with a set of orthophotos freely available on the Lombardia regional geoportal (https://www.geoportale.regione.lombardia.it/) dated 1954, 1975, 2003, 2015, 2018 and 2021, and the national geoportal (http://www.pcn.minambiente.it/mattm/) dated 1988, 1999, 2007, 2012. In addition, Google Earth images were considered as they represent the most recent and highest resolution data available. The active channel (Winterbottom, 2000; Nelson et al., 2013; Mandarino et al., 2020) including islands, hereafter defined as channel, was manually digitized as a polygon on each dataset at 1:2500 scale by a single operator. A reach characterized by homogeneous geomorphic features (Brierley and Fryirs, 2005; Rinaldi et al., 2015b), including the study area, was defined, and its planform evolution was investigated by computing area (CA), length (CL) and mean width (CW) of the channel. Moreover, the sinuosity (SI), braiding (BI) and anabranching (AI) indices (Mandarino, 2022 and references therein) were calculated to define the riverbed pattern following Rinaldi et al. (2016). At the site scale, the extent and position of the fluvial-terrace scarp investigated in this research was mapped following the above approach with reference to the channel. The scarp planform migration was assessed quantitatively through an overlay procedure (Mandarino et al., 2021b). Furthermore, 25 transects located perpendicular to and at a fixed distance of 25 m along the current smoothed scarp edge were considered to estimate the scarp edge retreat over time. According to previous studies (Surian et al., 2009) and considering the quality of images and the accuracy of digitizing, bank and scarp lines positioning was estimated to be affected by a positional error generally $\leq$5 m. On a more detailed scale, the single PS, SPS and major LS landforms, identified and characterized as described in Section 3.1, were systematically analysed and compared with available Google Earth images acquired from 2007 to 2021 to assess their temporal evolution. All these data and analyses were used to find a relation between fluvial-terrace scarp erosion and piping-sinkhole development. Lastly, a PS, SPS and LS database was created indicating for each landform the morphotype class, name, coordinates, diameter, depth, time of formation (where available), earliest documented date, and representative images. The full dataset of landforms was stored in a dedicated WebGIS that shows the PS-SPS-LS positions on a wide set of available base maps (years 1954, 1975, 1998, 2003, 2007, 2012, 2015, 2018, 2021). The WebGIS integration was developed with Web mapping Application of ARCGIS online (https://arcg.is/eKK4u). This type of visualization is fundamental to cover the study area with an appropriate detail (Maerker et al., 2019; Sartirana et al., 2020) as well as to clearly present overlapped landforms in time and space.

4. Results

4.1. Landform characterization and mapping

The observations and analyses led to the identification of two main classes of sinkholes which we interpret to be directly related to water flow in subsurface pipes. We term Piping-Sinkholes (PS) following Del Prete et al. (2008), a set of shallower sinkholes that are found on the terrace surface up to 30 m from the edge of the scarp and develop progressively further inland following the retrograding position of the escarpment (Fig. 5a, b, c and d). From statistical analysis (Fig. 6) they are typically about 4 m in diameter and 1.7 m deep, and we interpret them to be mainly related to piping phenomena occurring above clayey-silt layers a few meters depth from ground level, which can support perched water tables. The PS seemingly occur randomly (for a length of 435 m) on the river terrace scarp surface along the whole study area, but generally show a significant concentration in the southern part of the Casottole Belvedere area (Fig. 6).

The second class of piping-sinkholes, which we term Scarp Piping-Sinkholes (SPS), is generally larger and develop at the edge of the river terrace (for a length of 475 m) (Fig. 5e, g and Fig. 6, Appendices A, B). SPSs have a circular plan up to 50 m in diameter centred on or near the pre-collapse escarpment edge and are up to about 12 m deep when formed (Fig. 6). They are bowl to conical-shaped (Fig. 5e), and their perimeter, which is circular on the terrace, is reduced downslope. The perimeter does not intersect the base-flow channel border at the terrace scarp toe at the time of formation and displays a breach at the lower rim (facing the river), which represents the exit point of the collapsed material. Copious streams are seen to flow through the breach emerging from the central area after their formation. The highest concentration of large SPS landforms is found in the central part of the terrace scarp in the Belvedere area (Fig. 6, Appendix C), resulting in an overall gentler slope of the escarpment, while the adjacent areas to the N and to the S display a steeper escarpment dominated by slides and debris falls. Occasional, usually smaller SPSs are developed in the southern part of the study area. The most recent SPS recorded, SPS-18, was formed in August 2023 (Fig. 6, Appendix B). Unlike other large SPSs described, it was possible to document it very soon (a few days) after it collapsed, clearly detailing the abundant stream emerging from its centre and the large mass of debris spreading through the breach in the lower rim and forming a large debris cone outside the rim, containing large blocks, before this was destroyed by the river flow. This clear evidence of the SPS's mass wasting nature will be further described in the discussion section.

The PS, SPS, and main Landslide Scars (LS) (Fig. 5f) were initially plotted on high-resolution Google Earth Images available for 2007, 2012 and 2014–2021, in order to understand their temporal evolution. Fig. 6 synthesizes the main observations and shows the outlines and positions of all PS and SPS landforms, both current and past (eroded), as well as the active landslide scars and scarp margin, plotted on the most recent (March 2021) Google Earth image. The more recent (August 2023) SPS-18 outline is also shown on this image. Appendix C is focussed on the Belvedere area and shows the outlines and locations of the main landforms plotted on Google Earth images of 2007, 2012, 2016 and 2021. The landward migration of SPS and to a lesser extent PS positions with the retrograding of the scarp is clearly visible in this figure. The timing of PS and SPS formation, where documented or reasonably ascertainable, is consistently comprised between the months of July and October.

The PS, SPS, and LS positions and measurements, as described in Section 3.1 were stored in a GIS database and the mapped landforms plotted in a dedicated WebGIS. The WebGIS is freely accessible at the following link: https://unibicocca.maps.arcgis.com/apps/webappviewer/index.html?id=1ad7a2f0a00d44bb9b7fec6b25ad36d7.

4.2. Scarp geomorphological analysis

Dedicated field and laboratory analyses were conducted on the terrace scarp in order to fully characterize from a geomorphological, stratigraphic and textural point of view the escarpment and associated piping-sinkholes landforms. Initially, two geomorphological sketches were constructed along the scarp: the first directly on a SPS flank, and the second in a LS adjacent to a SPS (Fig. 7a and b). The sketches are useful to describe the geomorphological processes and associated landforms active on the slope. In particular, Fig. 7a shows how different SPSs activated in a time span of six years are now interconnected. In this part of the scarp the piping-sinkhole processes are presently inactive, but the inherited morphology leads to the formation of small gullies as well as metric-scale debris cones deposited on the scarp sediments.

As shown later, although the texture of the scarp is generally sandy, the slope inclination ensures that the scarp is now evolving principally due to the combination of slope-associated features as well as runoff processes like rill-interrill and small gully erosion. In addition, the geomorphological sketches clearly show how the grey basal level as well as other low-permeability levels such as the base of individual SPSs (e.g., SPS-10) are the seat of local water springs, that have directly influenced the SPS formation and their morphological evolution.

The marginal parts of the scarp (SVS) are more rectilinear and show different processes contributing to shape the scarp itself (Fig. 7b). This segment of the scarp was affected weeks earlier by two main landslides and a small SPS (LS-14 and 15 and SPS-13 of Appendix D), which were further shaped by a set of slope-associated processes contributing to create the specific features evidenced here. The scarp is largely sub-vertical, and a mantle of talus feed due to debris falls, debris cones and isolated fallen and toppled blocks can be observed on the scarp toe. Local springs can be seen to trigger small gullies directly on the talus feed transporting the unconsolidated materials and depositing them slightly downstream (Figs. 7b and 5g). These bodies are represented by metric-scale debris fans that are ephemeral and remodelled principally by the Ticino River flow with a marginal contribution of the rill-interrill runoff, well visible on the fan surface. While the scarp toe scouring by the river is the main origin of the landslides with consequent processes, the shaping of the top of the scarp can be directly associated with denudational and slope-associated processes that erode the scarp edge. This portion the SVS was re-activated in August 2023 with a major SPS (SPS-18), which is described in Sections 4.1 and 5.2.

In order to fully understand how the morphology of the scarp is associated with the local textural heterogeneity, two stratigraphic columns (Fig. 8) were constructed in correspondence with a significant SPS (i.e., SPS-10) and in the linear part of the scarp (Fig. 8a) in correspondence with LS-15. Samples collected in these two locations on the escarpment are representative of the two different geomorphological styles and show that the gentler slope area (SPS) consists of mainly unconsolidated sand/gravel (Fig. 8b), while the sediments in the steeper scarp areas (LS) are generally more cohesive and support steeper angles of repose (Fig. 8c). Although the textures of the different sedimentary layers are principally sandy, some specific silty layers can be detected and are directly related to the hydrological processes affecting the scarp. Fig. 8d (left) shows the stratigraphy sampled on SPS-10 with three layers (M4, M5 and M6) characterized by fine silty sand and silt grain size. In particular 2 m of silt (M6) is fundamental in the hydrodynamics of the scarp working as a low-permeability layer.

Another significant fine level, present along the base of the entire scarp and characterized by a greenish-grey colour (Gley1 4/5G_1 ref. Munsell soil colour chart), is represented by the M1-L1 clayey silt. As indicated by the grey colour this level straddles the mean river surface level and is often underwater. The top M1-L1 is characterized by frequent springs along the whole of the studied tract. In the rectilinear part of the scarp (Fig. 8c, d right) a thicker (3 m) layer of fine silt, named L6′ was observed. This fine horizon is not correlated with M6 and is well developed in the southern part of the study area. Elsewhere it is not laterally continuous, but heterotopic with a coarser silty sand layer (L6). This combination favours a scarp verticality and locally gives rise to fallen blocks. Finally, springs are frequently documented also between

Fig. 5. Piping-sinkhole and scarp erosion evidence in the study area. (a): inactive small PS (PS-6), 30 m from the river scarp. (b): recently formed PS near the scarp edge (PS-8). (c): large active PS close to the terrace scarp (PS-2). (d): terrace scarp retreat crosscutting the PS (PS-1). (e): SPS directly associated to the fluvial-terrace scarp. (f): path interrupted due to the fluvial-terrace scarp retreat. (g): linear scarp covered by talus on which springs can be observed. On the left, indicated by the arrow a small SPS (SPS-12) has directly formed on the scarp.

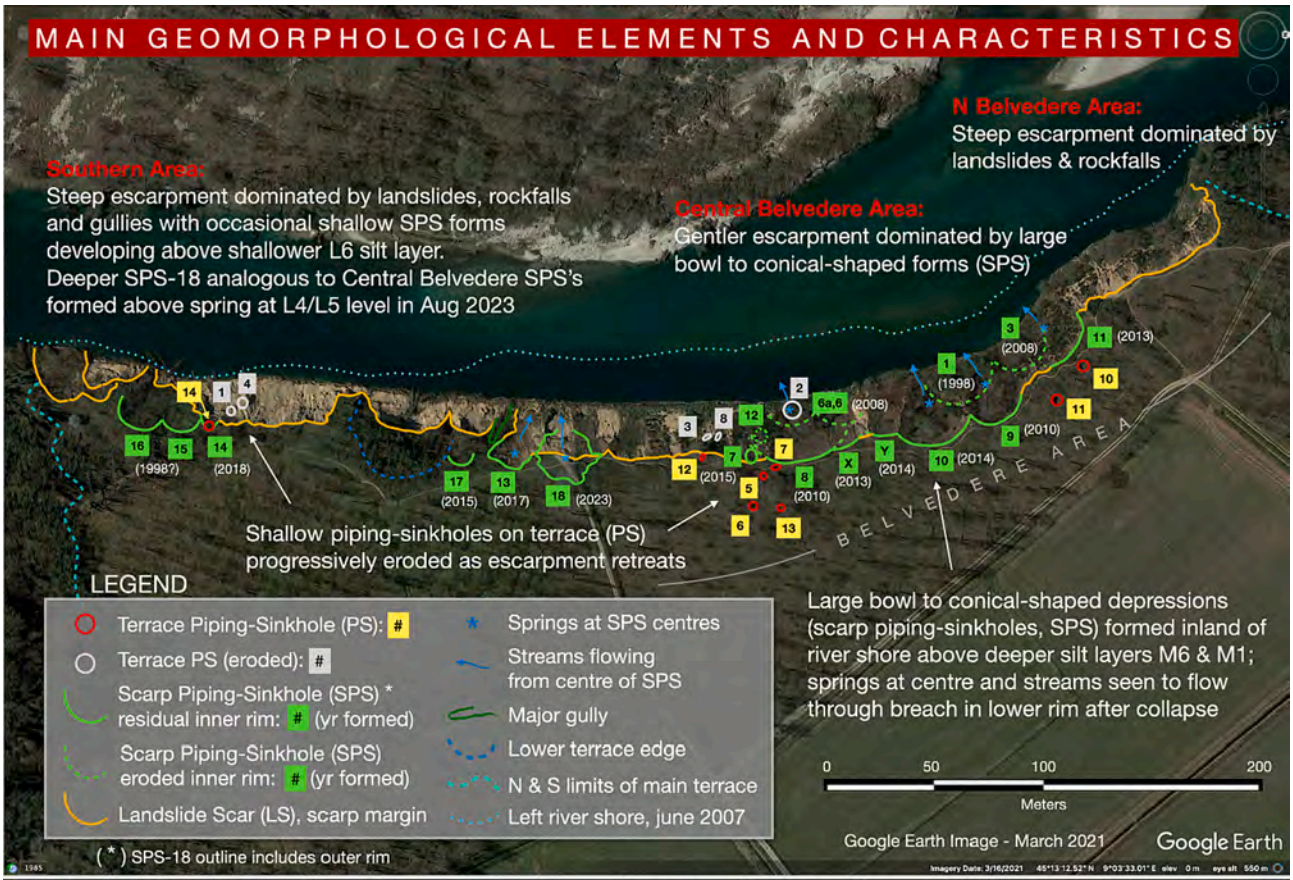

Landform type	Min. diameter	Max diameter	Mean diameter	Min. depth	Max. depth	Mean depth	Number of observed landforms
PS	2 m	10 m	4 m	0.7 m	2.5 m	1.73 m	13
SPS	5 m	50 m	23.52 m	2.5 m	12 m	6.25 m	22

Fig. 6. Main geomorphological elements and characteristics of the study area indicated on a 2021 Google Earth image (Google Earth, earth.google.com/web/). All terrace piping-sinkholes observed are shown, as well as surviving and past (now eroded) scarp piping-sinkholes (SPS).

L4 and L5 (Fig. 5g, Appendix D) and this level appears to play a major role in the development of the recent SPS-18. In the steeper scarp areas, the dominant erosional process is represented by scouring at the scarp toe, sometimes facilitated by strong underground water flow at the base of the escarpment as testified by abundant mud-rich springs emerging near the base, documented by drone images weeks and days before a major landslide (Appendix D).

4.3. Hydrological assessment

The hydrogeological assessment of the area is based on the publicly available data in the Lombardy Region portal (https://www.cartografia.servizirl.it/viewer32/index.jsp?config=config_caspita.json), and is synthesized in the two cross-sections of Fig. 9a and b, correlating the available stratigraphic logs with the scarp stratigraphy. Levels L1 and M1 can be easily correlated and are always easily recognizable on all photos and drone images, and their tops are the most frequent location of abundant springs. The sections show how both the higher M6 and L6 layers, less continuous than L1/M1, can support perched water tables as often documented by springs on the scarp, probably with associated piping, which can locally trigger SPSs or promote gully erosion. The local L4 layer, not represented in the sections, can also support local perched water tables, as well documented by springs in the LS-15/SPS-18 area. The presence of perched water tables is consistent with the free water level measured in local water wells in the Casottole area, (e.g., 86 m asl, or 2 m below surface in well Sw-A), where the regional aquifer top is found at about 68 m asl, as indicated by the regional piezometric map available in the Lombardy Region public portal (Eupolis Lombardia ter13016, Fig. 4 pag.5, February 2015). The perched water tables develop locally over laterally discontinuous low-permeability layers and can be fed by the main aquifer up-dip or by the surface network of natural and agricultural waterways, as well as by heavy or prolonged rainfall. To evaluate the soil infiltration capacity field experiments were conducted on three representative PS with a constant head-permeameter on the first soil horizon (0–30 cm). The test reveals an average infiltration capacity that varies from 12.9 to 17 cm/h, indicating high permeability values of the topsoil (ARPAV, 2011). The cross-sections realized starting from the available data show the asymmetry of this part of the Ticino valley. Indeed, the Ticino River today flows on the left side of the valley, undercutting the terrace scarp toe and eroding the study site.

Furthermore, field observation as well as the multi-temporal analysis conducted on orthophotos (Fig. 10) also indicate that piping-sinkholes are directly correlated to the riverbed morphological evolution. The oldest picture dated 1954 shows an anabranching trend of the river and no piping-sinkholes can be observed on orthophotos. Since the end of 1980s the change in the channel location and channel pattern (discussed in the next section), possibly combined with irrigation in fields behind the scarp, contributed to trigger piping phenomena bringing the scarp to be eroded by tens of meters.

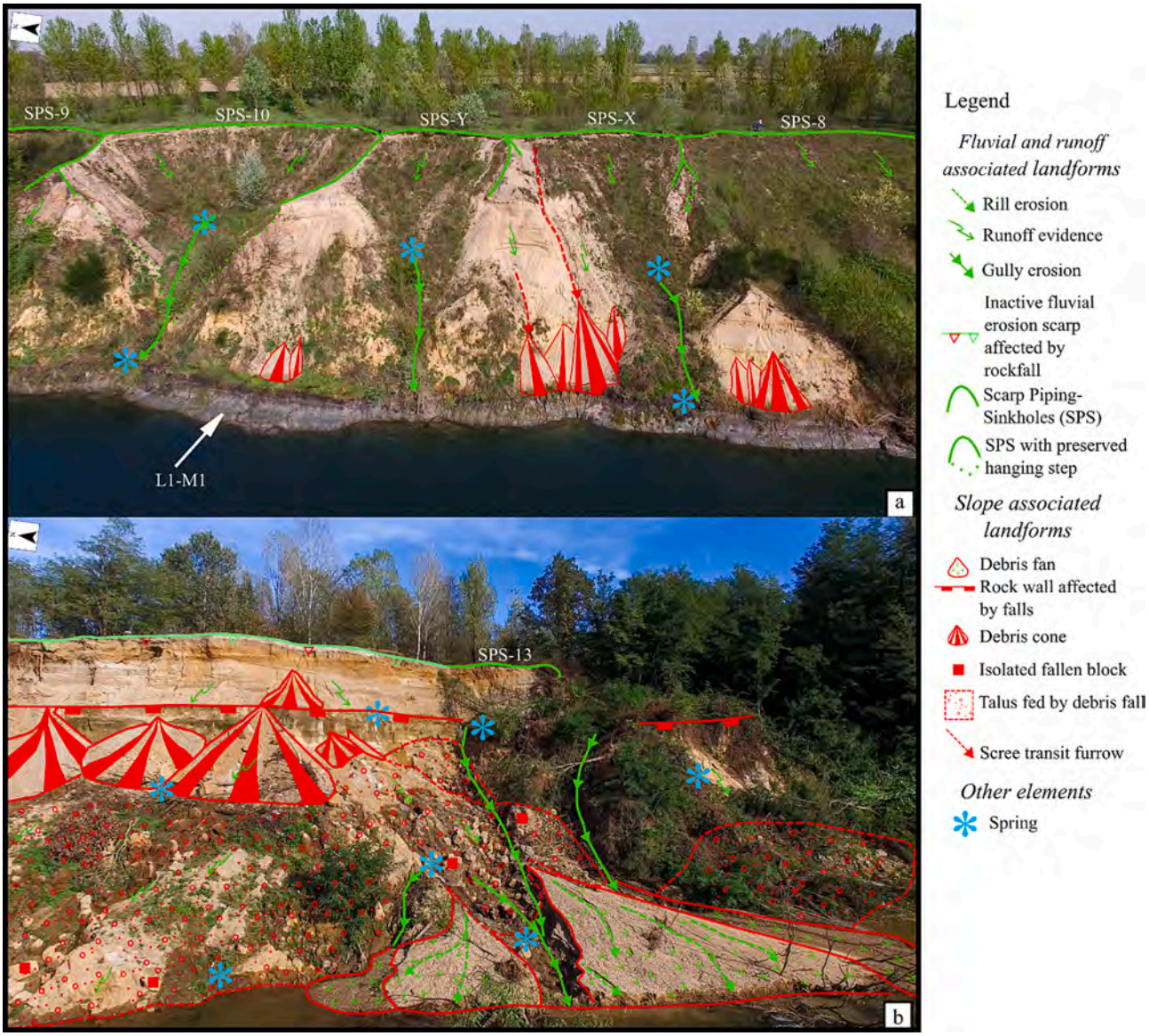

Fig. 7. Geomorphological sketch along the fluvial-terrace scarp. (a): Area characterized by different interdigitated SPSs. (b): Area where the scarp is sub-vertical (SVS) with a small SPS-13.

4.4. Channel and scarp multi-temporal evolution

Finally, the multi-temporal evolution of the scarp was evaluated. Table 1 shows the channel geomorphic features over time at a reach scale. The reach stretches from the highway bridge to a long-term stable farm (Fig. 10) and its length was between 4.5 and 4.6 km except for the most recent records which highlight an increase of about 840 m from 2015 to 2021 resulting in the present-day length of 5.4 km.

In contrast, CA ranged between 160 and 180 ha in the period 1988–2015 and recently decreased to some 130 ha, with an overall CA reduction of 64 ha from 1954 to 2021. These parameters are also reflected in CW, which progressively decreased, registering three major steps in periods 1954–1988 (−37 m, i.e., −8.6 %), 1988–1999 (−34 m, i.e., −8.7 %) and 2015–2018 (−132 m, i.e., −35.4 %). The CW overall reduced by 190 m (−44.1 %) from 1954 to 2021. SI remained constant for the whole period investigated except for the last years (i.e., since 2018) when a slight increase was noticed. BI experienced a marked decrease between 1975 and 2012, whereas a fluctuating trend in AI values over time was observed up to a decrease registered in 2018 and 2021. These indices (Table 1) allowed to classify the CP according to the basic (BRT) and extended (ERT) river typologies (Rinaldi et al., 2016). The channel was anabranching and, from 2018 onwards, wandering (Fig. 10).

The more detailed ERT classification allowed recognition of a transition from “Anabranching (high energy)/island-braided” pattern, observed until 2007, to “Anabranching (high energy)” pattern, observed in 2012 and 2015.

At the site scale (Fig. 11) the planform adjustments of the fluvial-terrace scarp touched by the channel that occurred over the time span considered, were defined (Table 2). The scarp area, intended as the planform area of the scarp, was 1.84 ha in 1954, 1.78 ha in 1975, 1.48 ha in 1988, 1.41 ha in 1999, 1.25 ha in 2003, 1.27 ha in 2007, 1.24 ha in 2012, 1.20 ha in 2015, 1.45 ha in 2018, and 1.48 ha in 2021. Major scarp retreats occurred in periods 1954–1975 (up to 60 m), 2007–2012 (up to 38 m), and 2015–2018 (up to 41 m) (Table 3). As shown in Table 3, in 2007–2012, 2012–2015, and 2018–2021 the retreat process affected larger portions of the scarp edge than In the other periods, with >60 % of transects registering scarp erosion. Localized scarp edge migration was observed in 1954–1975 and 2003–2007. Major terrace erosion associated with scarp retreat was documented in 1954–1975,

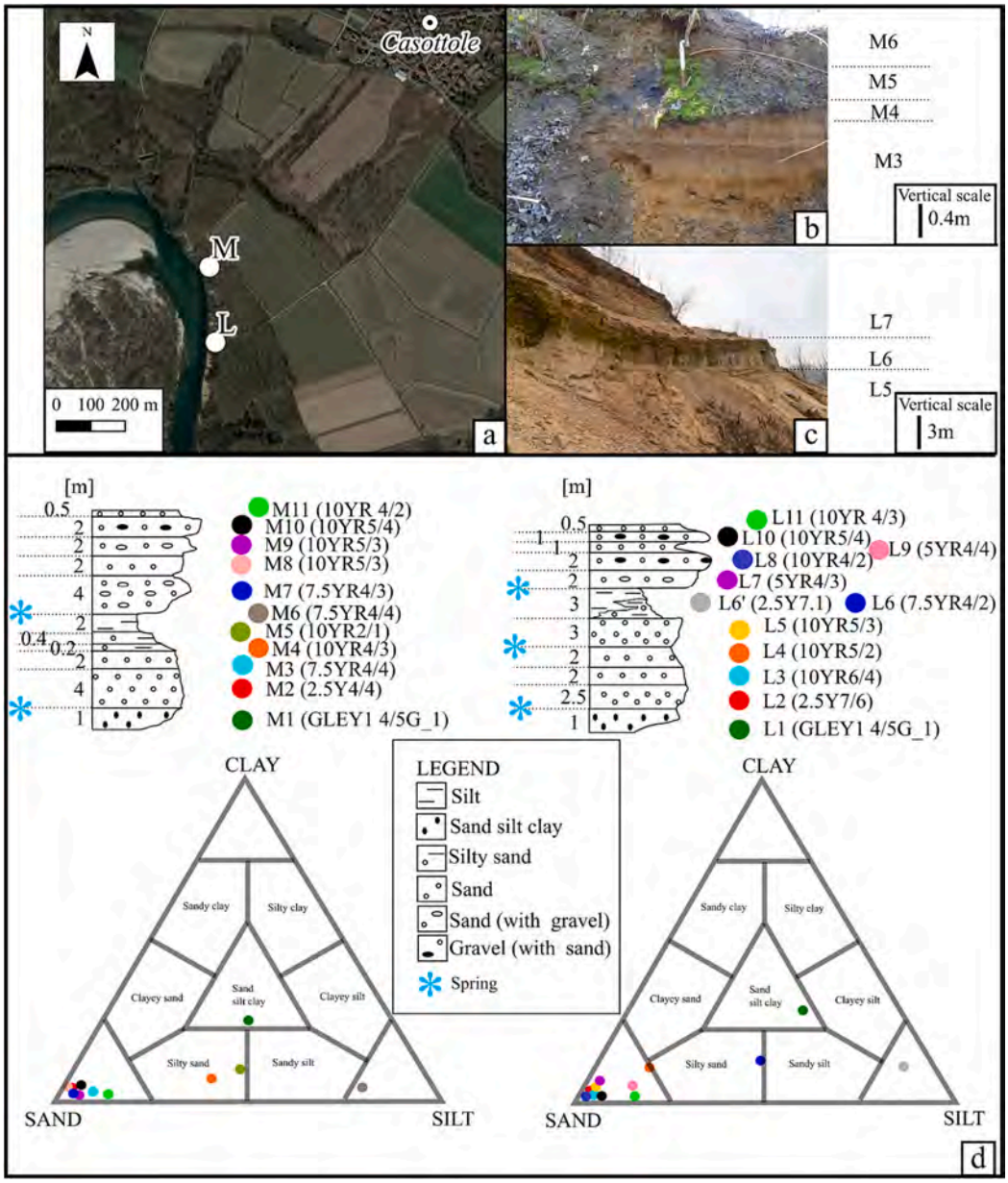

Fig. 8. Lithological characterization of the fluvial terrace scarp. (a): Location of stratigraphic profiles. (b): Overview of L5–7 in section L. (c): Overview of M3–6 in section M. (d): Stratigraphic columns with colour indication (Munsell Colour (Firm), 2010) grain size analysis plotted on Shepard triangular diagrams (Shepard, 1954).

2007–2012, and 2012–2015 (Table 2).

It is noteworthy that the highest terrace erosion rates (i.e., > 662 m^2yr^{-1}) were observed from the 2007–2012 period onwards. Before 2007 this rate was never higher than 299 m^2yr^{-1} (Table 2). Considering the whole period of 1954–2021, the maximum retreat was 79 m and this process affected substantially the whole scarp (Table 3). A reduction in scarp area was documented (Table 2), which corresponds to an overall increase in gradient. Only the 2003–2007 periods and after 2015 registered scarp area increase. The fluvial terrace scarp was already affected by evident erosion processes in 1988, as the channel shifted north-eastward between 1954 and 1988 (Fig. 10); from then to 2003, most of erosion processes occurred in the most downstream part of the scarp, while after 2003 instability was primarily observed at the Belvedere, namely, in the most upstream and middle parts of the scarp (Fig. 11).

The presence of both bare and vegetated areas over the scarp in each temporal image series and with differences in location over time, highlighted differences in the activity status of erosion processes affecting the scarp during the time span considered. The non-zero value of surface that changed from channel to scarp in 1988–1999 and 2015–2018 implies that erosion processes locally shaped a sediment deposit at the scarp toe. Referring to each period, the eroded scarp and the newly formed scarp, in terms of scarp area, ranged from 1.3 % (in 2003–2007) to 49.2 % (in 2007–2012) and 3.4 % (2003–2007) to 47.8 % (2007–2012), respectively (Table 2). In total, the eroded fluvial terrace was about 26,180 m^2.

5. Discussion

The outcomes revealed a complex geomorphological evolution experienced by the study area over the last decades through a multi-temporal and multi-scale analysis. The formation and evolution of PSs and SPSs were investigated in detail along with the river-induced erosion process affecting the terrace scarp. Although the two

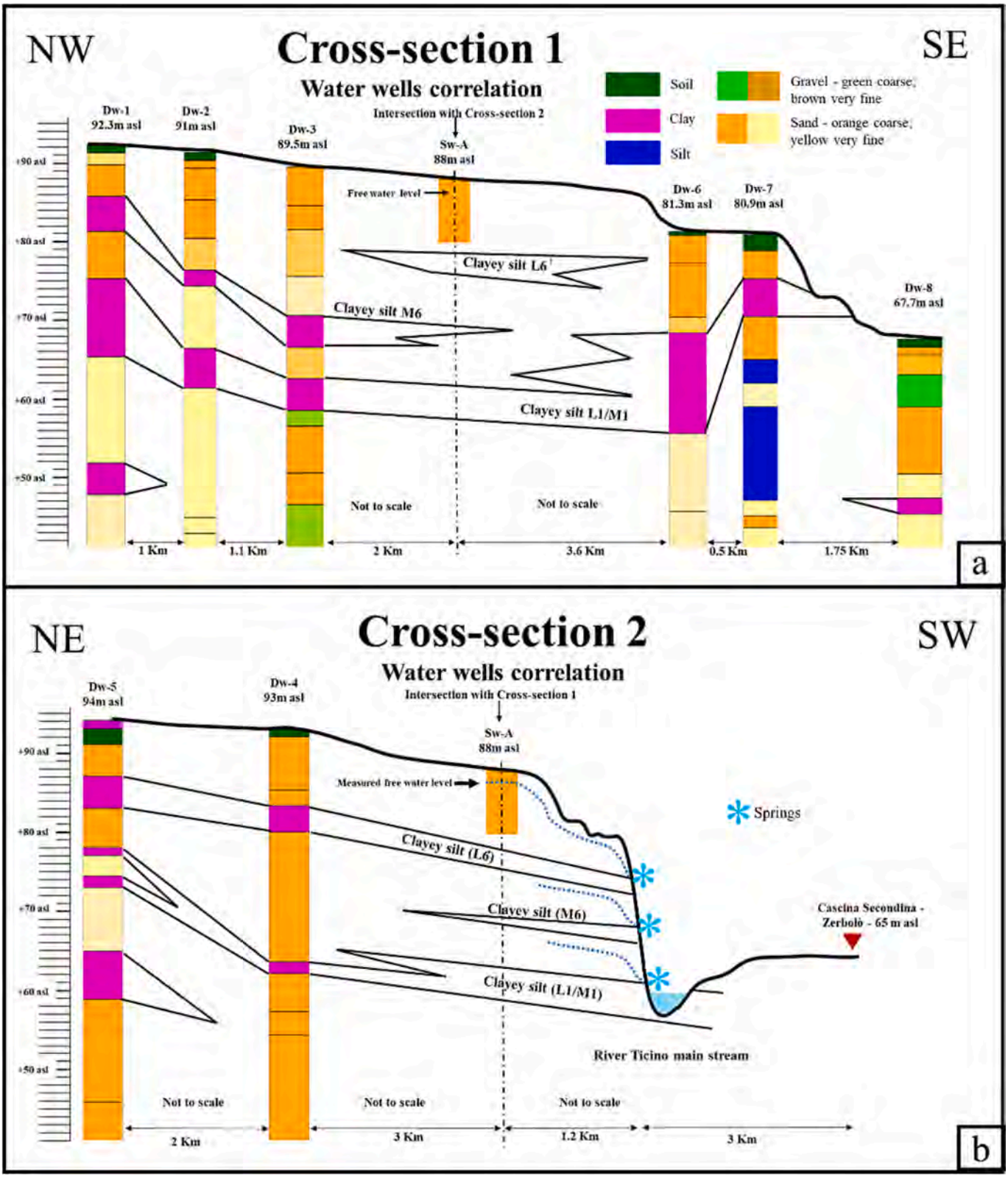

Fig. 9. Cross-sections (a) and (b) representing the lithological characteristics and layer correlation of the area. Cross-section (b) shows a scarp composite lithology derived from both L and M surveys to highlight the clayey-silt levels.

morphotypes are triggered by the same process i.e., piping, they present different morphologies and dimensions, and evolve in different ways in the area. A schematic conceptual-evolutionary model of PS, SPS and LS landforms is proposed in Fig. 12.

From field evidence it is clear how the lithological heterogeneity of the subsurface plays a fundamental role in the morphological evolution of the landforms. The Ticino River terrace shows the sedimentological characteristics typical of lowland river deposits with an alternation of fine and coarse sediments with the presence of heterogenic and heterometric lenses. It is recognized from literature (e.g., Jones, 1971;

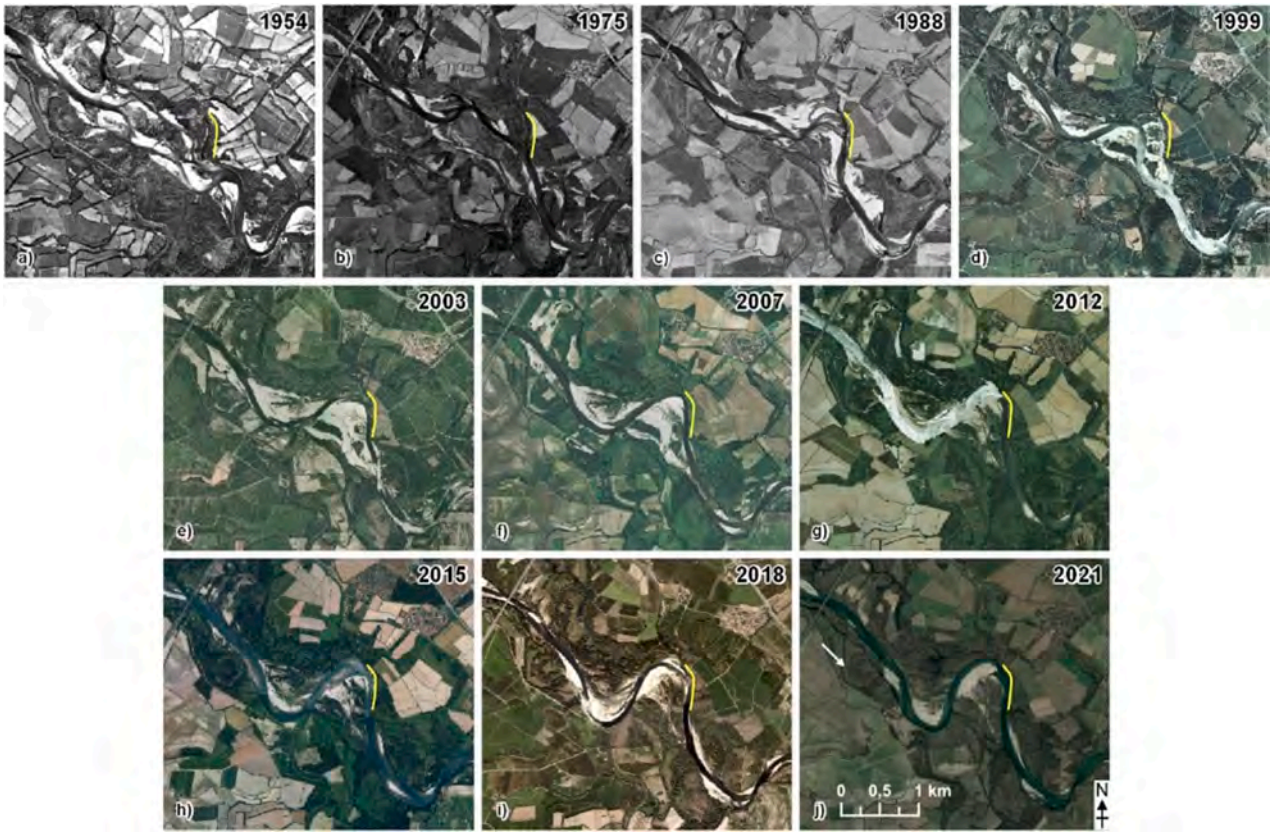

Fig. 10. Channel planform evolution from 1954 to 2021 at the reach scale. The white arrow indicates flow direction. The yellow line indicates the fluvial-terrace scarp investigated at the present-day location. Basemaps: orthophotos, see Section 3.4. (For interpretation of the references to colour in this figure legend, the reader is referred to the web version of this article.)

Table 1
(CL) channel length; (CA) channel area; (CW) channel width; (CP) channel planform features over time; (CP– BRT) channel pattern – basic river typologies; (CP – ERT) channel pattern – extended river typologies; (A) anabranching; (W) wandering; (Ahe/IB) anabranching (high energy)/island-braided; (Ahe) anabranching (high energy). (SI) sinuosity index, (BI) braiding, and (AI) anabranching Indices are dimensionless parameters.

Year	1954	1975	1988	1999	2003	2007	2012	2015	2018	2021
CL (m)	4511	4490	4562	4491	4513	4519	4602	4557	5291	5394
CA (ha)	194	184	179	161	164	166	163	170	127	130
CW (m)	430	410	393	359	363	367	354	372	240	240
SI	1.1	1.1	1.1	1.1	1.1	1.1	1.1	1.1	1.3	1.3
BI	1.6	1.6	1.4	1.4	1.4	1.4	1.1	1.1	1.3	1.1
AI	1.6	1.8	1.5	1.6	1.6	1.6	1.8	1.8	1.3	1.3
CP – BRT	A	A	A	A	A	A	A	A	W	W
CP – ERT	Ahe/IB	Ahe/IB	Ahe/IB	Ahe/IB	Ahe/IB	Ahe/IB	Ahe	Ahe	W	W

Hagerty, 1991) that variation of texture and porosity in alluvial banks can change hydraulic conductivity triggering piping phenomena. Moreover, another fundamental condition in the development of piping-sinkholes is the presence of a critical hydraulic gradient able to give to the water the necessary energy to remove particle (Jones, 1971). Although it is practically impossible to know in advance the exact hydraulic gradient at which piping begins (Hagerty, 1991), groundwater is clearly present in the study area because the Ticino River lies 20 m below the top of the terrace.

5.1. *Piping-sinkholes (PS)*

In the study area PSs sensu stricto (Fig. 5a, b, c, and d) develop on the top of the Ticino River terrace up to a few tens of meters from the scarp edge and are in average 1.7 m depth and 4 m wide. While we do not exclude the contribution of vertical flow of water caused by fluctuations of the water table and consequent upward propagation of cavities, as in the DPS of Nisio (2008), evidence in support of the mainly horizontal piping is that standing water has never been observed inside the PS.

Their morphological evolution is often related to the original location of the landform itself: in particular, those formed furthest from the edge of the scarp e.g., PS-06 or PS-13 (Fig. 6), after an initial growth become inactive (piping processes end after the collapse of the material), are smoothed by local runoff processes that directly act on the PS rim and are quickly filled by branches and leaves (Fig. 5a) (Nisio, 2003). PSs activated close to the edge of the river scarp are usually more active, due to the larger hydrodynamic gradient, until they are embedded in the scarp and destroyed due to the scarp retreat (e.g., PS-01, Fig. 5d). The piping-sinkholes developed on the terrace surface are distributed mainly along an E-W oriented belt in the central part of the study area (Fig. 6), and less frequently in the northern and southern areas. This may suggest preferential paths for groundwater flow and piping, e.g. as caused by buried fluvial paleo-channels. Their geometric characteristics support an origin by collapse due to piping and suffusion by subsurface water

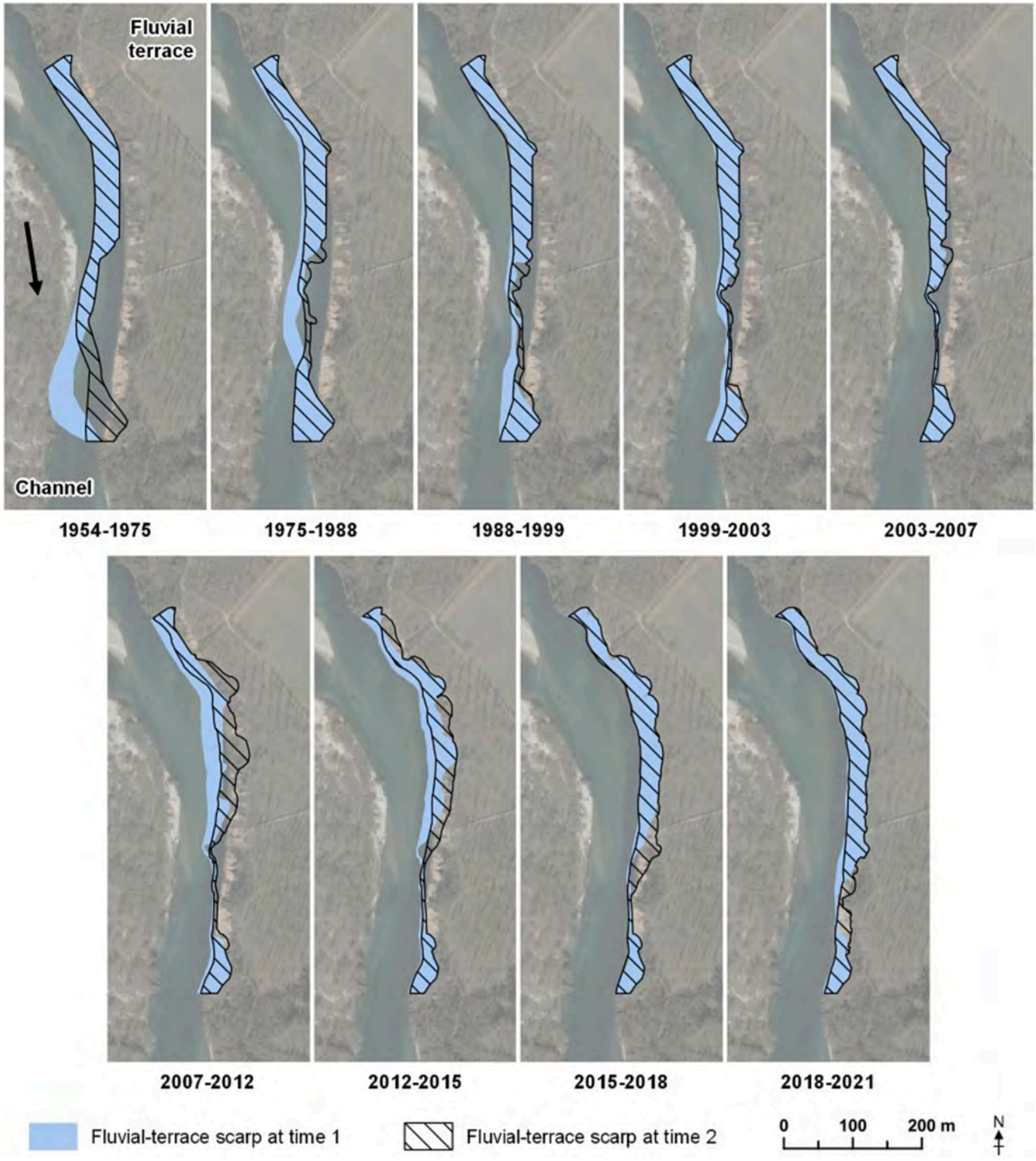

Fig. 11. Fluvial-terrace scarp location over the time span considered. Each sketch represents the comparison of consecutive data. Time 1 and time 2, respectively, correspond to the years reported below each sketch. The black arrow indicates flow direction; base map: Google Earth image dated back to 2021 (Google Earth, earth.google.com/web/).

flow over a relatively impermeable layer such as L6 at about 6 m below the surface. The patchy nature of these layers could also explain the irregular distribution of PSs developed further from the edge of the scarp. In general, the PS landforms have been observed to grow in width in the early months of their formation, and then remain substantially unaltered except for gradual infill by caving and erosion of the walls. One notable exception is PS-02, which is the largest of such landforms observed. It quickly reached its maximum size of about 10 m diameter and its position coincides with the centre of the large SPS-08 sinkhole formed about 2 years later. This could indicate a connection between the subsurface erosion effects that generated both landforms. The evolution of the PSs, especially those formed close to the fluvial scarp, could

Table 2
Planform adjustments over time of the fluvial-terrace scarp.

	No change (m^2)	From scarp to active channel (m^2)	From terrace to scarp (m^2)	From terrace to active channel (m^2)	From active channel to scarp (m^2)	Scarp area variation (m^2)	Eroded scarp (%)	Newly-formed scarp (%)	Eroded terrace (m^2)	Terrace erosion rate ($m^2\ yr^{-1}$)
1954–1975	13,090	5274	4726	1543	0	−548	28.7	26.5	6269	299
1975–1988	13,215	4601	1620	636	0	−2981	25.8	10.9	2256	174
1988–1999	12,125	2709	1698	196	240	−1011	18.3	12.3	1894	172
1999–2003	11,587	2477	885	0	0	−1592	17.6	7.1	885	221
2003–2007	12,317	156	427	0	0	271	1.3	3.4	427	107
2007–2012	6471	6274	5937	78	0	−337	49.2	47.8	6015	1203
2012–2015	8101	4305	3927	247	0	−378	34.7	32.6	4174	1391
2015–2018	11,690	340	2272	0	575	1932	2.8	16.3	2272	757
2018–2021	12,844	1694	1948	37	0	254	11.7	13.2	1985	662
1954–2021	1303	17,060	13,489	12,691	0	−3571	92.9	91.2	26,180	391

Table 3
Linear retreat of the fluvial terrace scarp edge over time. The scarp edge retreat corresponds to the length of the transect comprised between two consecutive scarp edge locations.

Period	Scarp edge retreat		Transects registering retreat (%)
	Max (m)	Mean (m)	
1954–1975	60	37.1	28
1975–1988	28	10.5	36
1988–1999	21	8.5	36
1999–2003	13	4.5	40
2003–2007	9	4.3	12
2007–2012	38	12.8	76
2012–2015	23	10.9	64
2015–2018	41	12.2	36
2018–2021	17	4.5	64
1954–2021	79	44.7	96

suggest that SPSs are an evolved stage of PSs, however, field observations do not support this hypothesis. Where it was possible to document it, the time of formation of all observed PS landforms was in late summer or autumn.

5.2. Scarp piping-sinkholes (SPS)

Conversely, SPSs present larger dimension (average diameter of 23.5 m with an average depth of 6.25 m), and a different distribution compared to PSs, representing another landform category found only on the river terrace scarp (Fig. 6, Appendices A, B). These landforms, especially the older, partially eroded ones, can be mistaken for landslide scars, but observation of the more recently formed ones show that they have a continuous sub-circular closed rim, broken only by a breach in its lower, outer part facing the river. The centre of the circle is situated at or near the previous position of the scarp edge, and the whole rim is contained within the terrace/scarp, i.e. it does not intersect the base-flow channel border at the terrace scarp toe. The flanks dip towards the centre, where streams emerge and flow through the breach into the river. These characteristics led us to interpret these as large sinkholes straddling the scarp edge, whose collapse was likely triggered by strong piping activity in the subsurface below the scarp edge, where the hydraulic gradient is highest. We interpreted the breach in the rim to be the exit point of the collapsed material, which was discharged into the river. However, initially, there was no direct evidence of this as available images were all referred to weeks or months after the SPS formation and did not show the collapsed material which had likely already been washed away by the river. In August 2023 a new SPS (SPS-18) was formed at the southern end of the Belvedere Area (Fig. 6, Appendix B). SPS-18 has all the characteristics of the previously mapped large SPS landforms, and shows a large volume of debris still inside the lower part of the sinkhole and overflowing through the rim breach into a large debris fan on the riverbank, including large blocks. We consider this as strong evidence of the sudden, mass wasting nature of these landforms. The springs in the SPS-18 centre emerge from the L4/L5 interface, the same horizon that generates springs in the nearby scarp and which appears to represent the base of this SPS.

SPS-18 has an irregular rim, compared to the smoother inner rims of other large SPS in the central Belvedere area (Fig. 6, Appendices A and C). We interpret this as mainly due to: (i) the more competent lithologies of the SPS-18 area, (ii) the irregular terrain intersected by the rim, including an elevated ballasted farm road which separates two slightly different height terrace portions. However the rim is relatively fresh and some smoothing by surface flow processes has yet to occur. South of SPS-18 is SPS-13, which was originally developed in August 2017 (Appendix D) and was reactivated in August 2023, giving rise to its own, finer and smaller debris fan (Appendix B). This SPS, like others in the southern part of the study area (14, 15, 16, 17), was generated above the L6 silt layer (Fig. 8), so they are smaller than the ones to the north where the bases are deeper in the section (see Section 5.3 below). SPS-13 also shows a more irregular outline and unlike most other SPS continued to evolve and enlarge by successive margin collapses.

The remaining SPS landforms, concentrated in the Belvedere area (Fig. 6, Appendix C), were mostly formed in the years 2012–2014, and appear to be all based on the M6 silt level (Fig. 8), with top about 10.5 m below surface. As with the PS landforms, SPSs were documented to have formed in late summer/autumn, in particular between July and October.

5.3. Piping and springs in relation to lithology and SPS formation

Overall, the different geomorphological styles displayed in the different parts of the scarp are attributed to lithological differences which influence the development of different landforms. The formation of SPSs is mainly correlated to piping above deep low-permeability layers. Three main relatively impermeable and competent clayey-silt layers occurring in the section can support water tables and induce piping phenomena where the hydraulic gradient increases towards the scarp. These are: (i) the L6 clayey silt layer, sampled in the southern area, (ii) the M6 clayey silt layer, sampled in the central area inside SPS-10 and (iii) L1/M1 basal clayey silt, present along the entire studied scarp. These layers are described in Section 4.2, through detailed geomorphological observations (Fig. 7) and analysis of the samples collected in representative locations of the scarp (Fig. 8). A copious spring was observed at the top of the L6 layer in SPS-13 (Appendix D, lower figure), with this level constituting the base of SPS landforms in the southern study area. Active springs were observed above the M6 level inside SPS-10 even 8 years after the SPS was formed. This level is thought to represent the main base of all the large SPS landforms in the Belvedere area (Fig. 6, Appendix C). Frequent, sometimes mud-rich springs seen above the L1/M1 level can contribute to the formation of SPS as well as landslides originating at the base of the scarp (see Section 5.4 below). Local textural variations of the sandy layers can also influence the water flow and generate piping processes. This is evident in the LS-14/15 and SPS-18/13 area, where numerous springs were

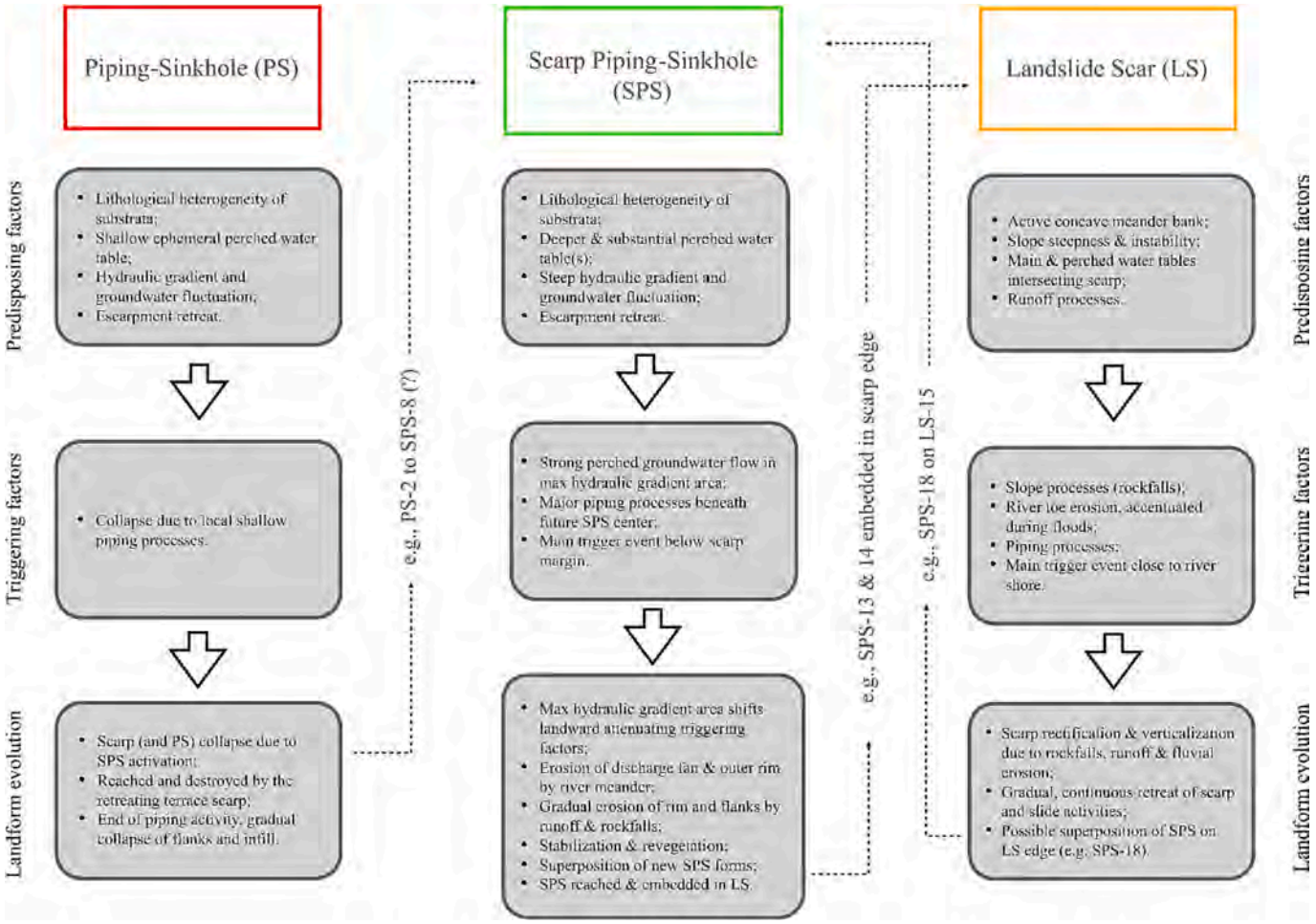

Fig. 12. Conceptual-evolutionary model of the landforms of the study area.

documented on the scarp and within SPS-18 corresponding to the L4/L5 interface (Fig. 5g, 7b, Appendices B, D). Although the L4 layer is barely located into the silty sand area of the Shepard diagram of Fig. 8, the textural difference with the L5 sand is sufficient to make this interface an important groundwater conduit.

Open piping exits (e.g., Hagerty, 1991) have not been observed on the Casottole scarp. This is explained by the loose nature of the overlying sediments which would quickly collapse onto any open cavity formed by flowing groundwater. However, strong indirect evidence of suffusion/piping was observed in the LS-15 area (Appendix D), where mud-rich springs exit the scarp near the top of L1, weeks before major slides took place (see Section 5.4 below). The above-referenced abundant stream at the top of L6, shown in the lower figure of Appendix D, is considered as indirect evidence of piping thought to have caused the formation of SPS-13. Close observation of such active exits was not possible also due to safety considerations.

5.4. Scarp piping-sinkholes vs landslide scars

As mentioned previously, SPSs can sometimes be confused with the large LSs affecting the terrace. However, careful observation of the evolution of these landforms shows that while for the SPSs the perimeter is always contained within the scarp at time of formation, for LSs, the circle described by the scar on the terrace always intersects the river shore. This is consistent with the SPSs being triggered by collapse below its centre, located at or near the scarp edge where the hydraulic gradient is highest, and the LSs being triggered by collapse very close to the river shore, i.e. caving of the foot of the scarp caused mainly by scouring of the toe. Piping can also have a role in the collapse at the foot of the scarp, as evidenced by the mud-rich springs emerging above the basal L1 silt layer weeks before major slides LS-14 and 15 collapsed (Appendix D). LSs are mainly developed where the scarp is steep or subvertical, i.e. in the northern Belvedere area and in the southern study area. Another distinguishing feature is that while the LS continue migrating landwards by continuous erosion of the scarp base, SPSs remain mostly fixed in their original positions for years after their formation, until gradually eroded by runoff and slope processes, or overrun by new SPSs, or reached and destroyed by river-induced scarp erosion (Fig. 12, Appendix C).

5.5. Evolution of SPS and LS landforms

The most recent processes affecting SPSs are associated with runoff and slope instability that tend to smooth the SPS rim in their upper part (Fig. 7a). The morphology of the scarp affected by SPSs is characterized by a set of semi-conical niches (Figs. 5e and 7a). Field observation of SPS morphology can indicate the relative age of the landforms themselves. SPS-10, activated in October 2014, preserves a sub circular rim hanging step from which the water can flow (Figs. 5e, 7a and Appendix A). The runoff that directly acts on the scarp as well as the river erosion at the toe of the fluvial scarp contributes to reshaping the SPS, removing the flanks and truncating it on the external part. The older SPSs, such as SPS-08, activated in October 2010, are today characterized by a smoother morphology, shaped by rills, minor gullies and landslides. The evolutionary mechanism of bank erosion affected by pipes is also described by Hagerty (1991) who highlights the interaction between different

processes in time. In our study, examples of the interaction of different processes in time are in the SPS-18/13 area, (Appendices B, D) where landslides LS-14 and 15 are later joined by SPS-13. Both of these gradually migrate inland until in 2023 SPS-18 is formed straddling the older LS-15 scarp margin and SPS-13 is reactivated. Further south, SPS-14 shows the original small sinkhole PS-14 which has later been included in the SPS, which is now itself included in a larger portion of the scarp edge migrating by successive landslides. SPS forms have been observed and mapped from 2004 to the present, the last major one being SPS-18, which was formed in late 2023. However, some such as SPS-01, were formed before this and are visible on the 1998 orthophoto. Alterations due to surface erosion are relatively minor, as is to be expected due to the limited runoff from the adjacent flat terrain and limited catchment area of the landforms themselves. River-induced scouring and undermining at the toe of the terrace scarp is presently responsible for the major modifications of landforms.

5.6. Ticino channel evolution and influence on SPS formation

Studying in detail the morphological evolution of the Ticino River channel over time, our quantitative analyses along with evidence from the imagery considered, revealed: (i) a loss of secondary channels, (ii) the stabilization of in-channel surfaces, and (iii) an increase in sinuosity, towards meandering. In particular, the wide secondary channels depicted in the 1954 image (Fig. 10) progressively became narrower or disappeared in the period 1954–1988. This resulted in the development of a main channel (Rinaldi et al., 2015a) and a few small secondary channels, often largely covered by forest tree species that further reduced from 1988 to 2021. In the meanwhile, the large bars characterizing the riverbed up to the early 2000s progressively turned into islands or modern floodplain leading to the CP – ERT variation from "Anabranching (high energy)/Island-braided" to "Anabranching (high energy)" between 2007 and 2012. The progressive annexation of in-channel stabilized areas to the adjacent floodplain that occurred over the last years, resulted in a narrower and more sinuous channel that became wandering. The lack of data concerning the channel vertical adjustments that occurred over the considered time span limited its investigation in this study. However, the described planform changes suggest that likely some riverbed incision occurred, as already documented elsewhere (e.g., Surian and Rinaldi, 2003; Cencetti et al., 2017; Pellegrini et al., 2008; Mandarino et al., 2019).

In this context, the Ticino River moved north-eastward up to the fluvial-terrace scarp toe, triggering lateral erosion processes that caused the scarp retreat and the fluvial terrace erosion, namely, the riverbed lateral mobility at a confinement element, for tens of meters in some decades. The river-induced erosion of the terrace scarp began between 1975 and 1988. Once the L1-M1 fine level was exposed, springs of perched groundwater started to crop out on the top of fine layers (initially L1-M1, and then L6-M6) triggering suffusion processes that rapidly generated SPS on the scarp. The earliest SPS are identifiable on the orthophotos of 1988. The outcomes concerning the scarp planform adjustments allow to argue that terrace erosion markedly prevailed during the whole period 1988–2021, and especially from 2004 to the present day, although differences existed in terms of type and spatial-temporal distribution of erosion processes affecting the scarp. The Ticino River played also an essential role in scarp undermining and deposit removal at the scarp toe by direct scouring. These processes were most likely associated with discharge variations. The formation of SPSs on the fluvial-terrace scarp as well as the PSs on the top of the terrace, are at present: (i) triggered by piping processes associated to local perched water tables and (ii) independent from river-related erosion. However, fluvial dynamics affect the evolution of the external part of the SPSs as well as the lower scarp. The outcomes revealed that fluvial dynamics were crucial as preparatory factors for SPS and PS modelling, because the progressive migration north-eastward of the channel, associated with the documented changes in pattern, resulted in the exposition of the fine-sediment levels.

5.7. Surface and groundwater influence on PS and SPS formation

This case study presents analogies with other cases documenting the formation of perched water tables and rapid subsurface flows to the riverbed triggered by floods that inundate the floodplain (Rinaldi et al., 2004; Wilson et al., 2007, and references therein). Here, perched water tables with flow towards the Ticino were observed (Figs. 7, 9, Annex A and D). However, their formation is totally independent from floods because the Ticino River is confined 20 m below the fluvial terrace surface. Their presence is rather primarily related to the regional configuration of the main aquifer whose top steeply slopes into the area from the NE towards the Ticino River, eventually reaching the level of the river at the base of the scarp. Any low-permeability layers encountered by the water descending through the section would constrain the downward flow creating perched water tables which would in turn concentrate the piping phenomena, more vigorously where the flow increases approaching the scarp. The dense and extended surface network of natural and irrigation waterways updip of the study area, together with heavy or prolonged rainfall and local water-intensive irrigation practices, such as rice field cultivation, can provide the refill and accentuate flow along the perched water tables and consequent piping. The timing of PS and SPS formation, in the late summer to autumn months, is consistent with the occurrence of maximum infiltration of surface water from irrigation or from late summer thunderstorms through desiccated soil into the perched water tables. As has been recognized by Hagerty (1991) the role of precipitation effects and overland flow as well as irrigation water or water stored in floodplains are key elements able to trigger piping processes. The lack of continuous or more frequent geomorphological monitoring of the escarpment have not allowed us to define the individual contribution of each possible driving factor on the evolution of erosional landforms. In contrast, this work clearly points out the overall effect that resulted from their combined action.

6. Conclusion

Piping-Sinkholes which outcrop along the lower Ticino River were studied in detail from a geomorphological point of view and have been characterized with field surveys and available remotely sensed images. The outcomes have been presented through a WebGIS service in order to freely share the landform positions, characteristics and associated processes. The study reveals for the first time the presence of piping-sinkholes in a hitherto unstudied area of northern Italy. Piping-sinkholes were classified on the basis of morphological evidence, in turn deeply related to the position of the landforms. Terrace Piping-Sinkholes (PS) were detected on the top of the river terrace, while piping-sinkholes located over the scarp were named Scarp Piping-Sinkholes (SPS). These landforms are activated by perched water tables of the higher semi-confined aquifer, whose origin can be associated with: (i) the lithological and hydrogeological conditions of the area, (ii) the presence of the extended surface network of natural and irrigation waterways updip of the study area, (iii) certain irrigation practices on the cultivated fields located on the river terrace close to the scarp, and (iv) heavy or prolonged rainfall in the area, which can contribute to refill the perched aquifers. In addition to the hydrogeological conditions, fluvial dynamics, and particularly the progressive migration north-eastward of the channel, were crucial as preparatory factors for SPS and PS occurrence and modelling, and today they contribute to shape the terrace-scarp. From this study it is possible to assert that by limiting water supply over the fluvial terrace significant benefit could be brought to minimize piping processes and associated landforms on the terrace surface and its scarp. The detection of piping-sinkholes on a retreating fluvial-terrace scarp and the adjacent fluvial-terrace surface represents a significant novelty in the scientific literature. Other types of erosional

landforms were described in association with riverbank erosion, such as cavities and gullies, and there are no available studies strictly focused on the modelling of river terrace scarps and the riverbed lateral migration towards a confining element. The outcomes from this research provide relevant information to enhance the overall knowledge of piping-sinkholes. Furthermore, they represent an important knowledge base to inform sustainable and effective measures for environmental management and hydrogeomorphic risk mitigation.

CRediT authorship contribution statement

A. Bosino: Writing – review & editing, Writing – original draft, Supervision, Methodology, Investigation, Data curation, Conceptualization. **A. Mandarino:** Writing – review & editing, Writing – original draft, Methodology. **M. De Amicis:** Software, Data curation. **F.F. Cazzini:** Writing – review & editing, Writing – original draft, Methodology. **D. Abu El Khair:** Writing – original draft, Data curation. **P. Flores:** Writing – review & editing, Writing – original draft, Supervision, Methodology, Data curation.

Declaration of competing interest

The authors declare that they have no known competing financial interests or personal relationships that could have appeared to influence the work reported in this paper.

Data availability

Data will be made available on request.

Acknowledgments

This research was conducted with the financial support of: (i) the RTDA-PON program (Research and Innovation 2014-2020, C6-G-32370-3) University of Milano-Bicocca, Department of Earth and Environmental Sciences and (ii) the Research funds of the University of Genova (100022-2022-AM-FRA_001). We thank the laboratories of University of Milano-Bicocca for grain size analysis, the GeoScape Company for providing field survey equipment, the Natural Park Parco Lombardo Valle del Ticino and the Morelli di Popolo family, owners of the area affected by the investigated landforms for their availability and for providing historical information.

Appendix A

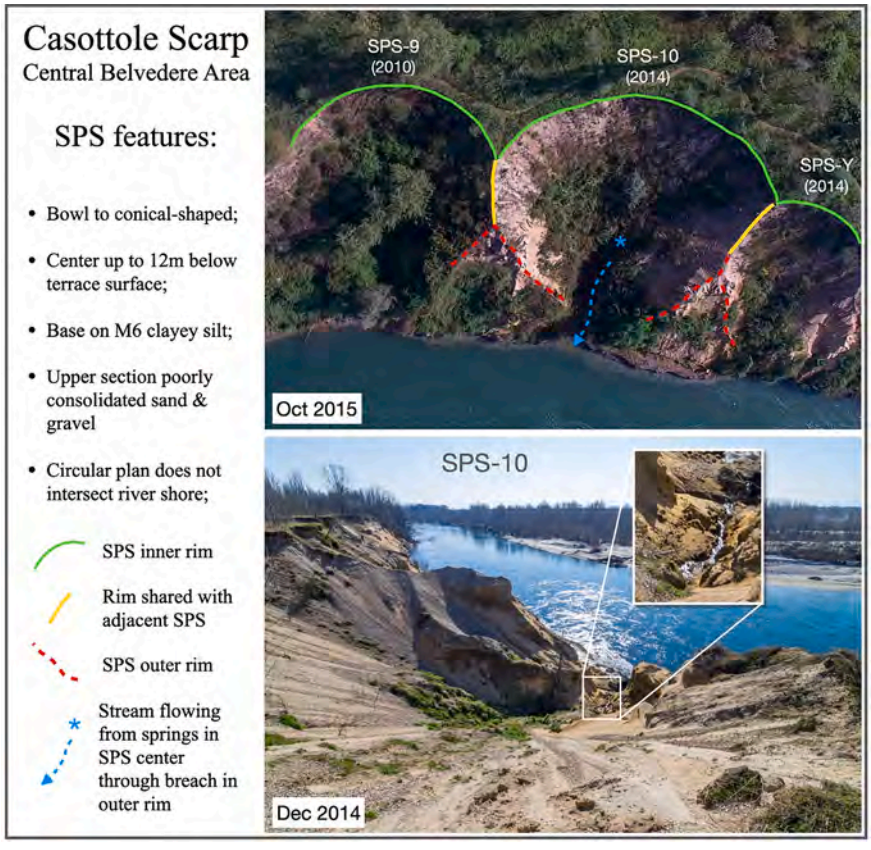

Fig. A.1. SPS in the central part of the scarp. Note the water outflow associated to low-permeability layers.

Appendix B

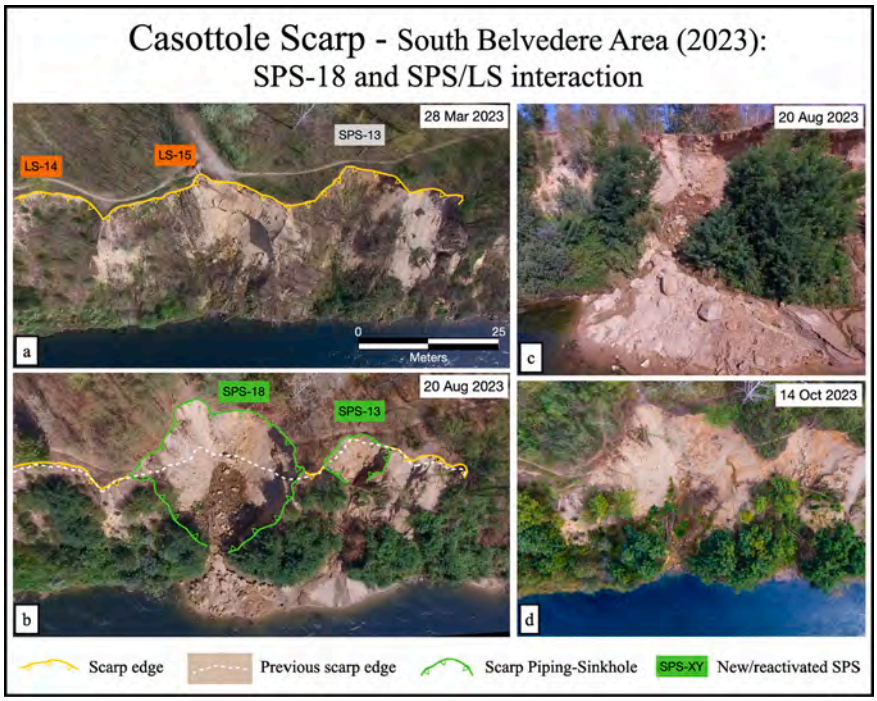

Fig. B.1. SPS-18 and SPS/LS interaction. (a): scarp edge includes LS-14 and 15 joined with remnants of 2017 SPS-13. (b): new SPS-18 on scarp edge and reactivated SPS-13 form distinct debris fans. (c): detail of SPS-18 debris fan. (d): fans destroyed by floods.

Appendix C

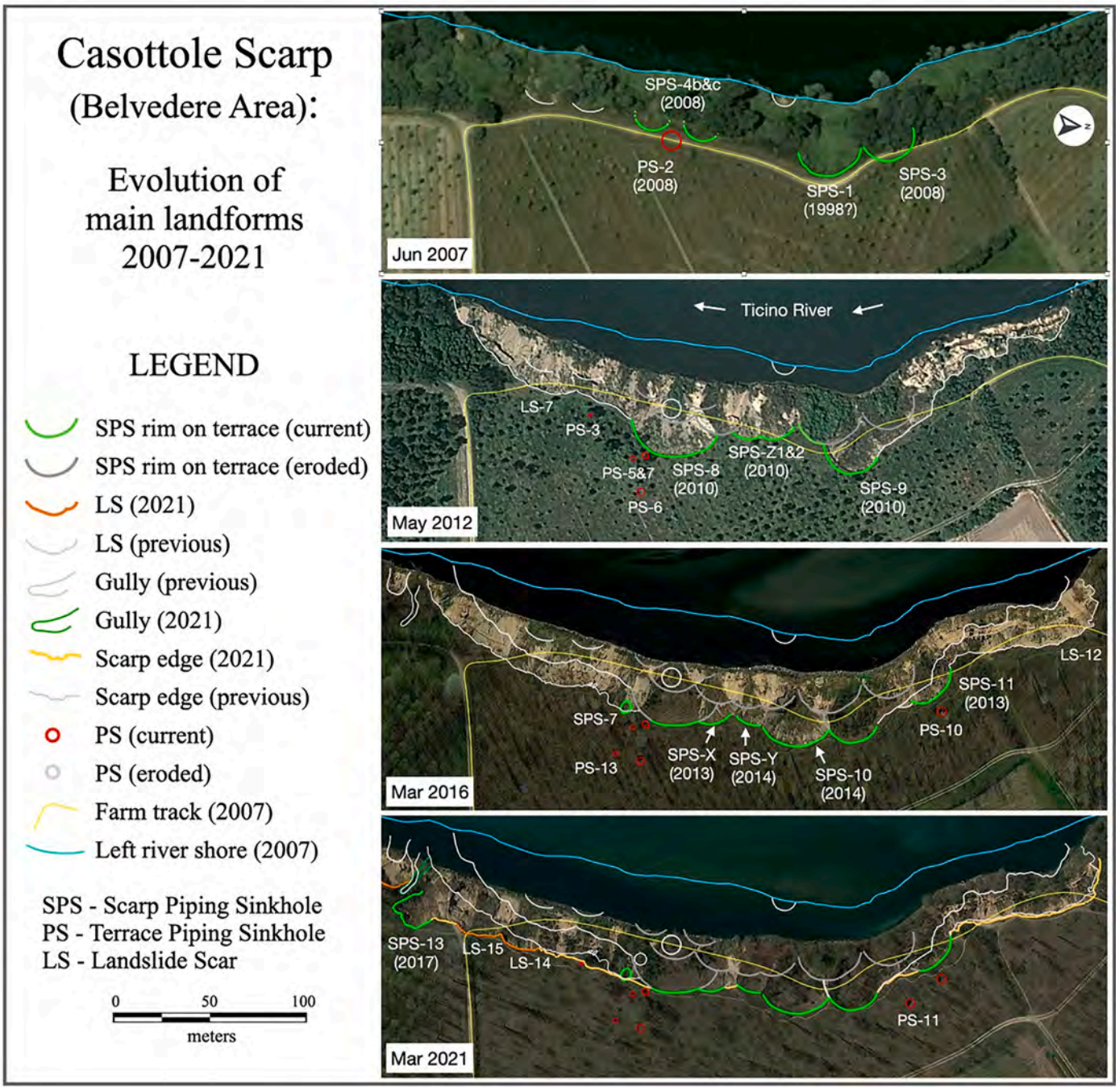

Fig. C.1. Evolution of main landforms between 2007 and 2021(Google Earth, earth.google.com/web/).

Appendix D

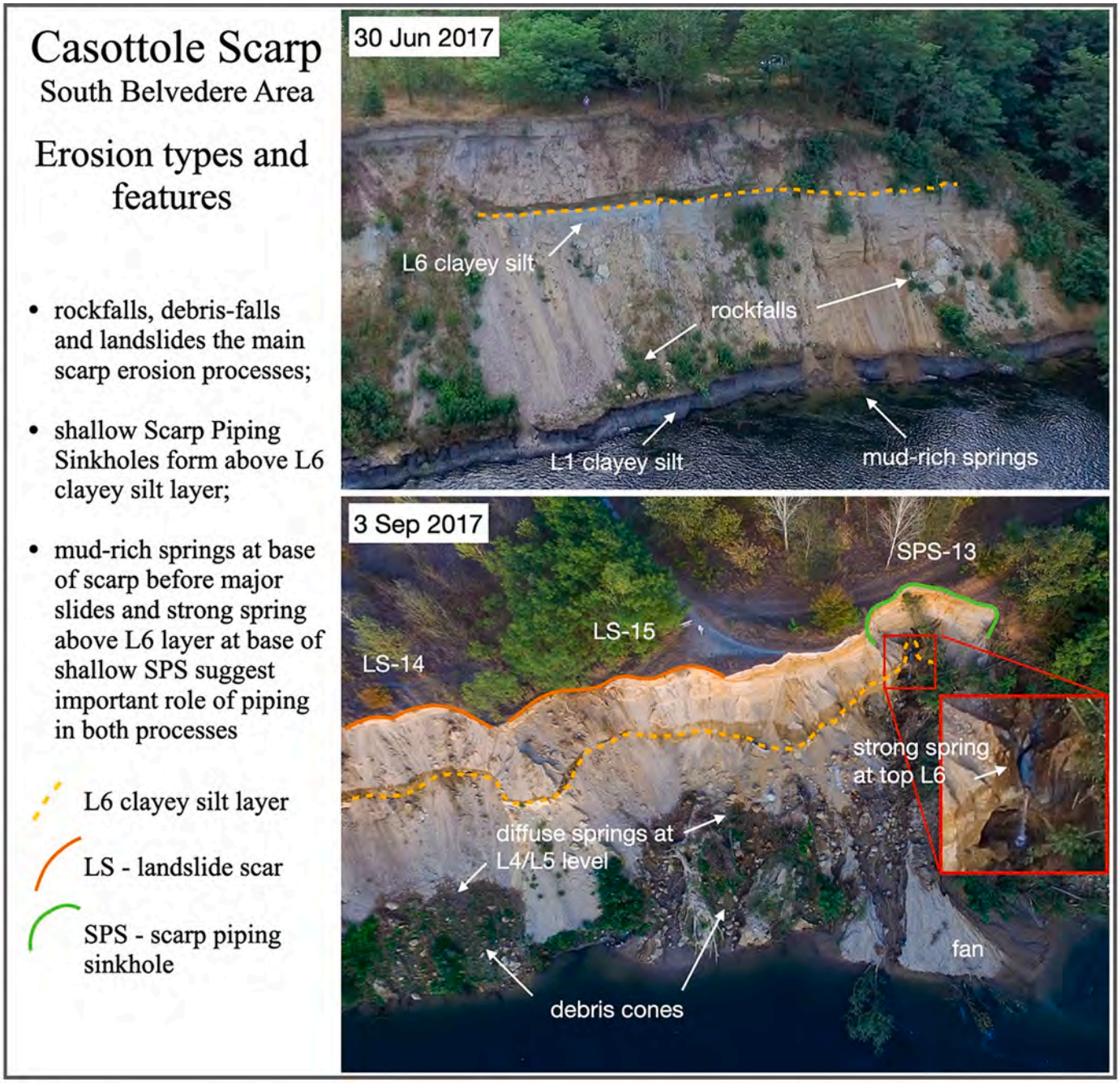

Fig. D.1. SPS and LS features and evolution in the south-central part of the scarp.

References

AdBPo, 2001. Autorità di Bacino del Fiume Po. Linee generali di assetto idraulico e idrogeologico – Fiume Ticino, 2021. https://pai.adbpo.it/index.php/documentazione-pai/.

Al-Halbouni, D., Holohan, E.P., Taheri, A., Schöpfer, M.P.J., Emam, S., Dahm, T., 2018. Geomechanical modelling of sinkhole development using distinct elements: model verification for a single void space and application to the Dead Sea area. Solid Earth 9, 1341–1373. https://doi.org/10.5194/se-9-1341-2018.

Amoozegar, A., 1989. A compact constant-head permeameter for measuring saturated hydraulic conductivity of the vadose zone. Soil Sci. Soc. Am. J. 53, 1356–1361. https://doi.org/10.2136/SSSAJ1989.03615995005300050009X.

ARPAV, 2011. Valutazione della permeabilità e del gruppo idrologico dei suoli del Veneto, 2011. ARPAV-Servizio Regionale Suoli.

Bates, R.L., Jackson, J., 1983. Dictionary of Geological Terms. American Geological Institute (571 pp.).

Beck, B.F., 1984. Sinkholes: their geology, engineering and environmental impact. In: Proceedings of the first Multidisciplinary Conference on Sinkholes, Orlando, FL. A. A. Balkema, Rotterdam, Netherlands (429 pp.).

Beck, B.F., Wilson, W.L., 1987. Karst hydrogeology: engineering and environmental applications. In: Proceedings of the Second Multidisciplinary Conference on Sinkholes and the Environmental Impacts of Karst, Orlando, FL. A. A. Balkema, Rotterdam, Netherlands (429 pp.).

Bernatek-Jakiel, A., Nadal-Romero, E., 2022. Can soil piping impact environment and society? Identifying new research gaps. Earth Surf. Process. Landf. 48 (1), 72–86.

Bernatek-Jakiel, A., Poesen, J., 2018. Subsurface erosion by soil piping: significance and research needs. Earth Sci. Rev. 185, 1107–1128.

Bernatek-Jakiel, A., Wrońska-Wałach, D., 2018. Impact of piping on gully development in mid-altitude mountains under a temperate climate: a dendrogeomorphological approach. Catena 165, 320–332.

Berry, L., 1970. Some erosional features due to piping and sub-surface wash with special reference to the Sudan. Geografiska Annaler. Series A. Phys. Geogr. 2 (2), 113–119.

Bettoni, M., Maerker, M., Sacchi, R., Bosino, A., Conedera, M., Simoncelli, L., Vogel, S., 2023. What makes soil landscape robust? Landscape sensitivity towards land use changes in a Swiss southern Alpine valley. Sci. Total Environ. 858, 159779.
Bianchini, S., Confuorto, P., Intrieri, E., Sbarra, P., Di Martire, D., Calcaterra, D., Fanti, R., 2022. Machine learning for sinkhole risk mapping in Guidonia-Bagni di Tivoli plain (Rome). Italy. Geocarto International 37 (27), 16687–16715.
Bosino, A., Omran, A., Maerker, M., 2019. Identification, characterisation and analysis of the Oltrepo Pavese calanchi in the Northern Apennines (Italy). Geomorphology 340, 53–66.
Bovi, R.C., Moreira, C.A., Rosolen, V.S., Rosa, F.T.G., Furlan, L.M., Helene, L.P.I., 2020. Piping process: genesis and network characterization through a pedological and geophysical approach. Geoderma 361, 114101.
Brierley, G.J., Fryirs, K.A., 2005. Geomorphology and River Management: Applications of the River Styles Framework. Blackwell Publishing.
Campobasso, C., Carton, A., Chelli, A., D'Orefice, M., Dramis, F., Graciotti, R., Guida, D., Pambianchi, G., Peduto, F., Pellegrini, L., 2021. Aggiornamento ed integrazioni delle linee guida della carta geomorfologica d'Italia alla scala 1:50.000 e banca dati geomorfologica, Quaderni serie III, Volume 13, Fascicolo I, Versione 2.0. ISPRA, Roma, 2021.
Caramanna, G., Ciotoli, G., Nisio, S., 2008. A review of natural sinkhole phenomena in Italian plain areas. Nat. Hazards 45, 145–172: Springer.
Cardarelli, E., Cercato, M., De Donno, G., Di Filippo, G., 2013. Detection and imaging of piping sinkholes by integrated geophysical methods. Near Surface Geophysics 12 (3), 439–450.
Cencetti, C., De Rosa, P., Fredduzzi, A., 2017. Geoinformatics in morphological study of River Paglia, Tiber River basin. Central Italy. Environmental Earth Sciences 76, 128.
Ceriani, M., Carelli, M., 1999. Carta delle precipitazioni medie, minime e massime annue del territorio alpino lombardo (registrate nel periodo 1891–1990). Milano, Regione Lombardia (in Italian).
Ciccacci, S., Galiano, M., Roma, M.A., Salvatore, M.C., 2008. Morphological analysis and erosion rate evaluation in badlands of Radiocofani area (Southern Tuscany–Italy). Catena 74, 87–97. https://doi.org/10.1016/j.catena.2008.03.012.
Clark, L.A., Wynn, T.M., 2007. Methods for determining streambank critical shear stress and soil erodibility: implications for erosion rate predictions. Trans. ASABE 50 (1), 95–106.
Colombo, L., Gattinoni, P., Cesareo, L., Consonni, M., 2015. Problemi di stabilità per le infrastrutture nelle aree interessate da cavità (occhi pollini) nei sedimenti pleistocenici della pianura lombarda. Memorie descrittive della Carta Geologica d'Italia 99, 315–326.
Consorzio Parco Ticino, 1998. Il Ticino. Studi e proposte sull'assetto idrogeologico e sull'uso del territorio della valle fluviale, p. 98.
Dapporto, S., Rinaldi, M., Casagli, N., Vannocci, P., 2003. Mechanisms of riverbank failure along the Arno River, Central Italy. Earth Surface Processes and Landforms: The Journal of the British Geomorphological Research Group 28 (12), 1303–1323.
Del Prete, S., Giulivo, I., Santo, A., 2008. Nuove ipotesi sulla formazione dei piping sinkhole in aree alluvionali: il caso della piana di Forino (Avellino, Campania). Il Quaternario-Italian Journal of Quaternary Sciences 21, 395–408.
Dell'Aringa, M., Giannecchini, R., Puccinelli, A., 2013. Small sinkhole-like features in alluvial plains: the example of Paganico (Lucca Plain, Italy). Nat. Hazards Earth Syst. Sci. 14, 41–51.
Dunne, T., 1990. Hydrology, mechanics, and geomorphic implications or erosion by subsurface flow. In: Higgins, C.G., Coates, D.R. (Eds.), Groundwater Geomorphology: The Role of Subsurface Water in Earth-surface Processes and Landforms, Special Paper, vol. 252. Geological Society of America, Boulder, CO.
Fairbridge, J., 1968. The Encyclopedia of Geomorphology. Reinhold, New York (1295 pp.).
Fannin, R., Slangen, P., 2014. On the distinct phenomena of suffusion and suffosion. Géotechnique Letters. 4 https://doi.org/10.1680/geolett.14.00051.
Farifteh, J., Soeters, R., 1999. Factors underlying piping in the Basilicata region, southern Italy. Geomorphology 26 (4), 239–251.
Froese, J.C., Cruse, R.M., Ghaffarzadeh, M., 1999. Erosion mechanics of soils with an impermeable subsurface layer. Soil Sci. Soc. Am. J. 63, 1836–1841.
Gutiérrez, F., 2016. Sinkhole hazards. In: Oxford Research Encyclopedia of Natural Hazard Science.
Hagerty, D.J., 1991. Piping/sapping erosion. I: basic considerations. J. Hydraul. Eng. 117 (8), 991–1008.
Hagerty, D.J., Spoor, M.F., Ullrich, C.R., 1981. Bank failure and erosion on the Ohio River. Eng. Geol. 17, 141–158.
Hooke, J.M., 1979. An analysis of the processes of river bank erosion. J. Hydrol. 42 (1–2), 39–62.
Jones, A., 1971. Soil piping and stream channel initiation. Water Resour. Res. 7 (3), 602–610.
Jones, J.A.A., 1994. Soil piping and its hydrogeomorphic function. Cuaternario y Geomorfología 8 (3–4), 77–102.
Kottek, M., Grieser, F., Beck, C., Rudolf, B., Rubel, F., 2006. World map of the Köppen-Geiger climate classification updated. Meteorol. Z. 15 (3), 259–263.
La Licata, M., Bosino, A., Bettoni, M., Maerker, M., 2023. Assessing landscape features and geomorphic processes influencing sediment dynamics in a geomorphologically highly active Mediterranean agroecosystem: the upper Val d'Arda case study (Northern Apennines, Italy). Geomorphology 433, 108724.
La Vigna, F., 2016. Groundwater and civil protection, what the Italian for "hydrogeological risk" should mean. Acque Sotterranee-Italian Journal of Groundwater 5 (4).
La Vigna, F., Teoli, P., Mazza, R., Leoni, G., and Capelli, G., 2013. Regional sinkhole susceptibility maps: The Latium Region case (central Italy). Mem. Descr. Carta Geol. D'It. XCIII (2013), pp. 277–284 figg. 4, tabb. 2.
Maerker, M., Schillaci, C., Melis, R.T., Kropáček, J., Bosino, A., Vilímek, V., Mussi, M., 2019. Geomorphological processes, forms and features in the surroundings of the Melka Kunture Palaeolithic site. Ethiopia. Journal of Maps 15 (2), 797–806.
Mandarino, A., 2022. Morphological adjustments of the lower Orba River (NW Italy) since the mid-nineteenth century. Geomorphology 410, 108280.
Mandarino, A., Maerker, M., Firpo, M., 2019. Channel planform changes along the Scrivia River floodplain reach in northwest Italy from 1878 to 2016. Quat. Res. 91 (2), 620–637.
Mandarino, A., Pepe, G., Maerker, M., Cevasco, A., Brandolini, P., 2020. Short-term GIS analysis for the assessment of the recent active-channel planform adjustments in a widening, highly altered river: the Scrivia River. Italy. Water 12 (2), 514.
Mandarino, A., Luino, F., Faccini, F., 2021a. Flood-induced ground effects and flood-water dynamics for hydro-geomorphic hazard assessment: the 21–22 October 2019 extreme flood along the lower Orba River (Alessandria, NW Italy). J. Maps 17 (3), 136–151.
Mandarino, A., Pepe, G., Cevasco, A., Brandolini, P., 2021b. Quantitative assessment of riverbed planform adjustments, channelization, and associated land use/land cover changes: the Ingauna alluvial-coastal plain case (Liguria, Italy). Remote Sens. 13 (18), 3775. https://doi.org/10.3390/rs13183775.
Marchetti, M., 2002. Environmental changes in the central Po Plain (Northern Italy) due to fluvial modifications and anthropogenic activities. Geomorphology 44 (3), 361–373.
Monroe, W.H., 1970. A Glossary of Karst Terminology. U.S. Geol. Surv, Water Sup.
Munsell Color (Firm), 2010. Munsell Soil Color Charts: With Genuine Munsell Color Chips. 2009 Year Revised. Munsell Color, Grand Rapids, MI.
Nelson, N.C., Erwin, S.O., Schmidt, J.C., 2013. Spatial and temporal patterns in channel change on the Snake River downstream from Jackson Lake dam, Wyoming. Geomorphology 200, 132–142.
Nisio, S., 2003. I fenomeni di sprofondamento: stato delle conoscenze ed alcuni esempi in Italia centrale. Il Quat (Ital J Quat Sci) 16, 121–132.
Nisio, S., 2008. I sinkhole: problemi terminologici, meccanismi genetici, classificazione. Memorie descrittive della carta geologica d'Italia, Volume LXXXV, 2008, pp.17–32 figg.4.
Nisio, S., Salvati, R., 2004. Fenomeni di sprofondamento catastrofico. Proposta di classificazione applicata alla casistica italiana. In: Proceeding: State of the Art on the Study of Sinkhole Phenomena and Role of the National and Local Government in the Territory Administration. Rome, 20–21 May 2004, pp. 573–584.
Nisio, S., Caramanna, G., Ciotoli, G., 2007. Sinkholes in Italy: first results on the inventory and analysis. Geol. Soc. Lond. Spec. Publ. 279 (1), 23–45.
Nisio, S., Del Prete, S., Guarino, P.M., Iovine, G., Parise, M., Santo, A., 2008. I fenomeni naturali di sinkhole nelle aree di pianura italiane. Mem Descr. Carta Geol. d'It LXXXV (2008).
Okeke, C.A., Azuh, D., Ogbuagu, F.U., Kogure, T., 2020. Assessment of land use impact and seepage erosion contributions to seasonal variations in riverbank stability: the Iju River. SW Nigeria. Groundwater for Sustainable Development 11, 100448.
Parise, M., Vennari, C., 2013. Chronological catalogue of sinkholes in italy the first step toward a real evaluation of the sinkhole hazard. In: 13th Multidisciplinary Conference on Sinkholes and the Engineering and Environmental Impacts of Karst, pp. 383–392 (Carlsbad (New Mexico, USA), May 6-10, 2013).
Parise, M., Vennari, C., Guzzetti, F., Marchesini, I., Salvati, P., 2013. Preliminary outcomes from a catalogue of natural and anthropogenic sinkholes in Italy, and analysis of the related damage. Rend. Online Soc. Geol. Ital. 24, 225–227.
Parker, G.G., 1964. Piping: A Geomorphic Agent in Landform Development of the Drylands, vol. 65. International Association of Scientific Hydrology, Wallingford, UK, pp. 103–113.
Pellegrini, L., Maraga, F., Turitto, O., Audisio, C., Duci, G., 2008. Evoluzione morfologica di alvei fluviali mobili nel settore occidentale del bacino padano. Italian Journal of Quaternary Sciences 21, 251–266.
Pilla, G., 2010. Gli acquiferi di pianura della provincia di Pavia: origine e qualità della risorsa. Assessorato alla tutela ambientale settore tutela ambientale. Centro Copie di Enrico Riganti, San Martino Siccomario (2010).
Rinaldi, M., Casagli, N., 1999. Stability of streambanks formed in partially saturated soils and effects of negative pore water pressures: the Sieve River (Italy). Geomorphology 26 (4), 253–277.
Rinaldi, M., Casagli, N., Dapporto, S., Gargini, A., 2004. Monitoring and modelling of pore water pressure changes and riverbank stability during flow events. Earth Surf. Process. Landf. 29 (2), 237–254.
Rinaldi, M., Belletti, B., Comiti, F., Nardi, L., Bussettini, M., Mao, L., Gurnell, A.M., 2015a. The Geomorphic Units Survey and Classification System (GUS). Deliverable 6.2, Part 4, of REFORM (REstoring rivers FOR effective catchment Management), a Collaborative Project (Large-scale Integrating Project) Funded by the European Commission Within the 7th Framework Programme Under Grant Agreement 282656.
Rinaldi, M., Surian, N., Comiti, F., Bussettini, M., 2015b. A methodological framework for hydromorphological assessment, analysis and monitoring (IDRAIM) aimed at promoting integrated river management. Geomorphology 251, 122–136.
Rinaldi, M., Gurnell, A.M., Del Tánago, M.G., Bussettini, M., Hendriks, D., 2016. Classification of river morphology and hydrology to support management and restoration. Aquat. Sci. 78, 17–33.
Römkens, M.J.M., Prasad, S.N., Helming, K., 1997. Effect of negative soil water pressures on sediment concentration in runoff. In: SSY, Wang, Langendoen, E.J., Shields, F.D. (Eds.), Managementof Landscapes Disturbed by Channel Incision. The University of Mississippi, Oxford, MS, pp. 1002–1007.
Sartirana, D., Rotiroti, M., Zanotti, C., Bonomi, T., Fumagalli, L., De Amicis, M., 2020. A 3D geodatabase for urban underground infrastructures: implementation and

application to groundwater management in Milan metropolitan area. ISPRS Int. J. Geo Inf. 9 (10), 609.
Scorpio, V., Aucelli, P.P.C., Giano, S.I., Pisano, L., Robustelli, G., Rosskopf, C.M., Schiattarella, M., 2015. River channel adjustments in Southern Italy over the past 150 years and implications for channel recovery. Geomorphology 251, 77–90. https://doi.org/10.1016/j.geomorph.2015.07.008.
Servizio Geologico D''Italia, 1967. Carta Geologica D'Italia, Foglio 59 Pavia, Roma.
Sharp, J., 2016. Glossary of Hydrogeological Terms. The University of Texas, Austin, Department of Geological Sciences.
Shepard, F.P., 1954. Nomenclature based on sand-silt-clay ratios. J. Sedlm. Petrol. 24, 151–158.
Simon, A., Curini, A., Darby, S., Langendoen, E.J., 1999. Streambank mechanics and the role of bank and near-bank processes in incised channels. In: Darby, S.E., Simon, A. (Eds.), Incised River Channels: Processes, Forms, Engineering and Management. John Wiley and Sons, New York.
Strini, A., 2004. Erosione Sotterranea e sprofondamenti nell'alta pianura Lombarda: gli "Occhi Pollini". Stato dell'arte sullo studio dei fenomeni di sinkholes 665–675.
Strzałkowski, P., 2019. Sinkhole formation hazard assessment. Environ. Earth Sci. 78 (1), 9.
Surian, N., Rinaldi, M., 2003. Morphological response to river engineering and management in alluvial channels in Italy. Geomorphology 50, 307–326.
Surian, N., Rinaldi, M., Pellegrini, L., Audisio, C., Maraga, F., Teruggi, L., Turitto, O., Ziliani, L., 2009. Channel adjustments in northern and central Italy over the last 200 years. In: James, L.A., Rathburn, S.L., Whittecar, G.R. (Eds.), Management and Restoration of Fluvial Systems With Broad Historical Changes and Human Impacts. Geological Society of America Special Paper 451. Geological Society of America, Boulder, CO, pp. 83–95.
Tharp, T.M., 1997. Mechanism of formation of cover collapse sinkholes. In: Proceedings of the 6th Multidisciplinary Conference of Sinkhole and the Engineering and Environmental Impact of Karst. Balkema, Rotterdam, The Netherlands, pp. 29–36.
Thorne, C.R., Abt, S.R., 1993. Analysis of riverbank instability due to toe scour and lateral erosion. Earth Surf. Process. Landf. 18 (9), 835–843.
Waltham, T., Bell, F., Culshaw, M., 2005. Sinkholes and Subsidence. Praxis Publishing Springer.
White, W.B., 1988. Geomorphology and Hydrology of Karst Terrains. Oxford University Press, New York.
Williams, P., 2004. Dolines. In: Gunn, J. (Ed.), Encyclopaedia of Cave and Karst Science. Taylor and Francis Group, New York, London, pp. 304–310.
Wilson, G., 2011. Understanding soil-pipe flow and its role in ephemeral gully erosion. Hydrol. Process. 25 (15), 2354–2364.
Wilson, W., Moore, J., 1998. Glossary of Hydrology. American Geological Institute (248 pp.).
Wilson, G.V., Periketi, R.K., Fox, G.A., Dabney, S.M., Shields, F.D., Cullum, R.F., 2007. Soil properties controlling seepage erosion contributions to streambank failure. Earth Surface Processes and Landforms: The Journal of the British Geomorphological Research Group 32 (3), 447–459.
Wilson, G.V., Wells, R., Kuhnle, R., Fox, G., Nieber, J., 2018. Sediment detachment and transport processes associated with internal erosion of soil pipes. Earth Surf. Process. Landf. 43 (1), 45–63.
Winterbottom, S.J., 2000. Medium and short-term channel planform changes on the Rivers Tay and Tummel, Scotland. Geomorphology 34, 195–208.